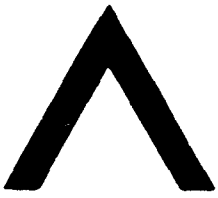

ARTECH CORP.
14554 Lee Road • Chantilly, Virginia 22021-1632
(703) 378-7263 • Washington, D.C. Metro 968-TEST • Fax (703) 378-7274

SUPERHARD COATINGS FOR BEARINGS

Fred Ordway
Charles Feldman

November 5, 1990

Final Report

Contract No. DAAL04-88-C-0020

Prepared for

U. S. Army Materials Technology Laboratory
Watertown, Massachusetts 02172-0001

ARTECH Report J8931-FR

SUMMARY

The object of the work was to produce cubic boron nitride (cBN) coatings on types 17-4 and 440 stainless steel used in spherical rod end bearings. The coatings were formed on these and other substrates by ion-assisted physical vapor deposition. Infrared absorption spectra of coatings on silicon substrates showed the presence of the cubic modification of BN. Indentation measurements, by a special technique that separates the contribution of the film from that of the substrate, demonstrated high microhardness values. Motor-driven feedthroughs were installed in the vacuum chamber in preparation for the coating of spherical bearing components. Sample coupons submitted to the sponsor were found by a scratch test technique to show poor adhesion to the stainless steel. The remainder of the program was therefore devoted to improvement of the coating-substrate bond. Tensile bond strength values as high as 6,700 lb/in.^{2} were attained. Some time after completion of the experimental work, however, it was found that the the coatings were cracking into minute fragments and spalling off the substrates. The failure mechanism remains to be determined.

CONTENTS

FIGURES

TABLES

SUPERHARD COATINGS FOR BEARINGS

CONTRACT NO. DAAL04-88-C-0020

FINAL REPORT

ARTECH Report J8931-FR

1. INTRODUCTION

1.1 Background

This is the final report on a project sponsored by U. S. Army Materials Technology Laboratory (MTL), Watertown, Massachusetts, as a Phase I contract under the Small Business Innovative Research program. The work extended over more than the intended six-month contract period because of the relocation of ARTECH's laboratory into a new facility, with attendant requirements for rewiring, inspection, and approval of equipment. Further delays were caused by breakdown of insulators in the ion and electron guns, which required rebuilding of both units.

The object of the work was to test the superhard coating of cubic boron nitride (cBN), previously developed by ARTECH, on the spherical bearing surfaces of large rod end bearings, such as might be used in helicopter swash plate linkages.

1.2 Properties of Boron Nitride

Boron nitride is described as a superhard coating for a number of reasons. Boron itself is the second hardest element, next to diamond; on the Mohs scale, boron is listed as 9.3 compared to diamond as 10. Boron is easy to deposit in the pure state and forms excellent adherent films. It forms compounds with both chromium and iron, which should promote its adhesion to stainless steel. The addition of nitrogen to boron moves the hardness closer to diamond providing the diamondlike cubic structure is achieved. This has been done by a number of workers including those at ARTECH [1,2,3,4]*. Boron nitride is resistant to common acids and alkalies. It is stable in air to at least 700°C. It can be formed by gas phase reactions and it can also be formed in vacuum.

When formed by an ion-assisted vacuum deposition process, the BN layers can be very pure, as indicated by a secondary ion mass spectroscopy (SIMS) analysis performed during earlier work at ARTECH [1]. Hydrogen content in the deposited films, for example, was only about 0.16%.

Diamondlike carbon, on the other hand, is difficult to deposit in pure form by thermal evaporation of the element, and is usually deposited from a gaseous phase by an ion beam assisted process, r-f plasma decomposition, or sputtering. The carbon films generally contain hydrogen, oxygen, and other

* Numbers in brackets indicate references listed in the bibliography, section 7.

impurities[5]. Some of the hardest films are known to contain up to 10% of hydrogen; the structure apparently requires hydrogen to satisfy bonding requirements. (This behavior is similar in some respects to that of amorphous silicon-hydrogen alloys.) Under heat (400°C), and perhaps wear, the diamond-like carbon coatings tend to lose their hydrogen and decompose. Diamond oxidizes when heated in air, of course, making its usable temperature range under ordinary circumstances more restricted than that of boron nitride. Tribological properties such as coefficient of friction have been found to depend on humidity[5]. The rate of wear of the coating has been found to vary with the hydrogen content in the film. Diamond-like carbon coatings do not adhere well to stainless steel.

The tribological properties of boron nitride films about 2 μm thick have recently been explored[2]. The coefficient of friction between a rounded pin and flat plate with boron nitride coated surfaces was found to be approximately equivalent to that of hard ceramics such as silicon carbide.

2. COATING PROCESS

2.1 Description

The boron nitride layers were formed by simultaneously impinging boron atoms and nitrogen ions on a substrate. This process is sometimes termed "ion-assisted deposition." Depositions were carried out in a nitrogen partial pressure of about 8×10^{-5} torr.

The nitrogen ions were accelerated in an ion gun by an electric potential of 2-3 kV. The ion gun was positioned so that the maximum ion current was approximately in the center of the substrate holder.

The boron was evaporated from a water-cooled crucible, in which it was heated by an electron beam at a power of 0.3-0.4 kW. The flux of boron atoms and that of nitrogen ions were adjusted so that an approximate stoichiometric ratio would be present at the substrate. The arrangement of the ion gun and the boron source is illustrated in figure 1. Schematic diagrams of the ion gun and its power supplies are shown in figure 2.

The substrates were supported by a stainless steel frame with openings for nine one-inch square substrates, but only three or four of these substrates received adequate ion bombardment. Ion collectors (Faraday cups, figure 3), to measure the beam current, and glass substrates for subsequent measurement of film thickness occupied other substrate positions. The ion collector was maintained by a battery at -18 V with respect to its grounded shield. The current produced by ions striking the 1-cm^2 aperture was read on a Keithley electrometer.

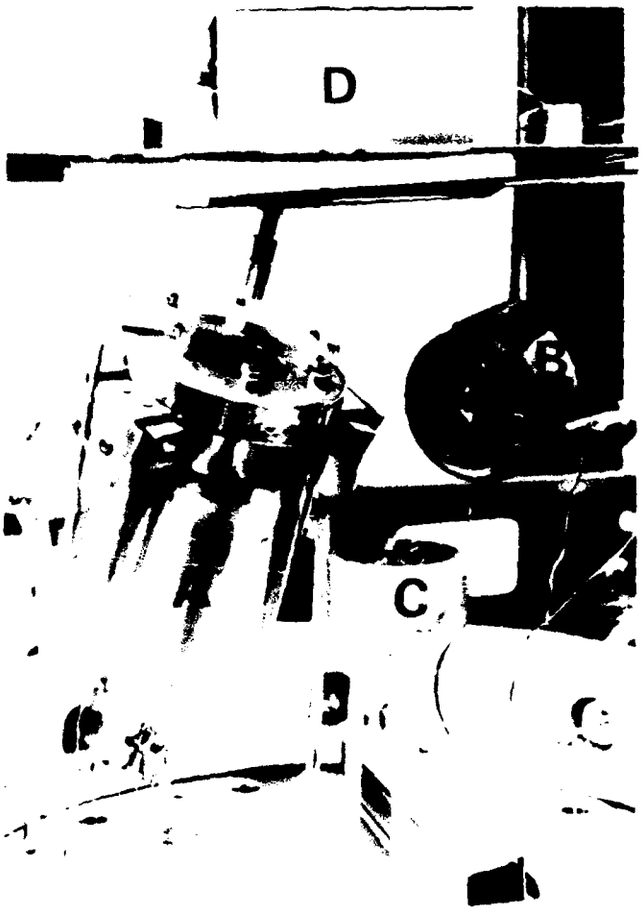

Figure 1. Apparatus for producing boron nitride coatings: (A) nitrogen ion gun, (B) electron beam gun with deflector electrode, (C) boron evaporation crucible, (D) substrate heater resting on the flat substrate holder.

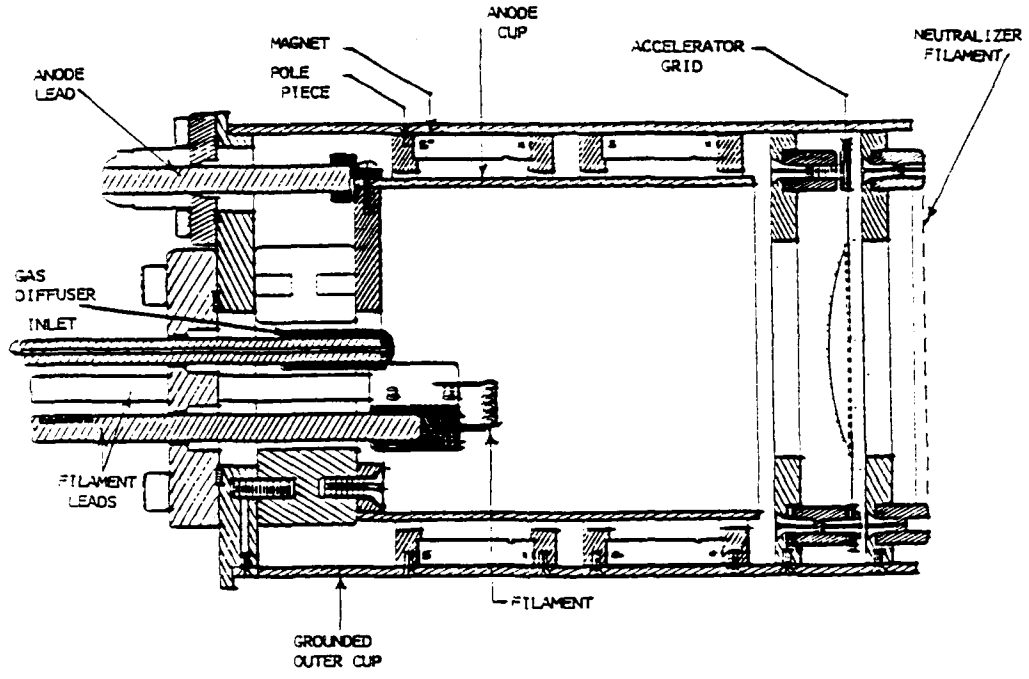

(A)

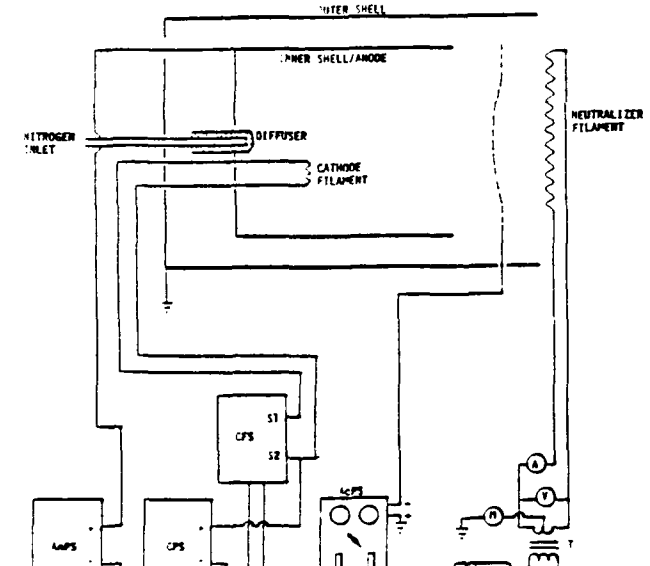

AnPS - Anode Power Supply
Kilovolt Corporation model KV5-500S
0-5 kV filtered dc, 0-500 mA

CPS - Cathode Power Supply
Consolidated Vacuum Corporation model LC-031
0-5 kV full-wave rectified ac, 0-750 mA

CFS - Cathode Filament Supply
MRC Manufacturing Corporation model V43001
Variable autotransformer and stepdown transformer
Original transformer with 10-V, 25-A secondary
replaced by one with 22-V, 18-A secondary S1, S2

AcPS - Accelerator Power Supply
NJE Corporation model H-35
0-10 kV filtered dc, 0-50 mA

Neutralizer Filament Supply

U - 7.5-A variable autotransformer
T - stepdown transformers connected to provide
a 44-V, 18-A center-tapped secondary
A - ac ammeter, 0-10 A
V - ac voltmeter, 0-25 V
M - dc milliammeter, 0-50 mA

(B)

Figure 2. (A) Structure of ion gun; (B) arrangement of power supplies.

Test coupons of 17-4 and 440 stainless steel were cut 4-6 mm thick from 1-in. square bars by bandsawing and were ground and polished by standard metallographic laboratory techniques. During most runs, a stainless steel coupon for evaluation of hardness and adhesion and silicon substrates for measurement of infrared spectra as well as hardness were placed in the substrate holder. An example of the arrangement of substrates is shown in figure 4 for deposition run BN56.

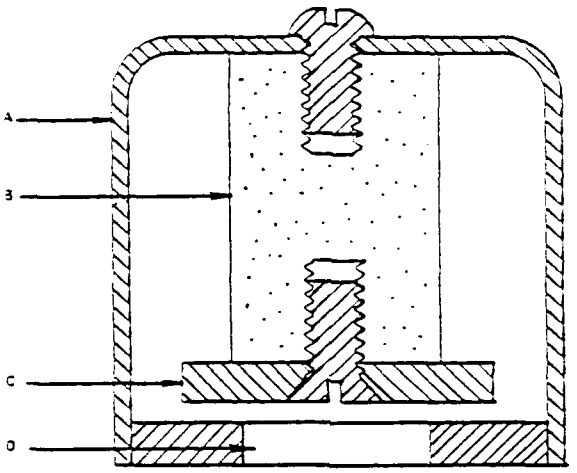

Figure 3. Cross section of the shielded ion collector: (A) grounded stainless steel cage; (B) ceramic insulator; (C) collector plate, 3/4 in. square, held at -18 Vdc; (D) aperture, 0.444 in. in diameter, in 1-in. square base.

	A	B	C
1	Glass	Glass	Ion Collector
2	Ion Collector	SS440 Electro-Polished	SS440 Mechanical Polished
3	SS440 Electro-Polished	SS440 Mechanical Polished	Silicon Wafer

Front

Figure 4. Arrangement of substrates in holder for deposition BN56.

Substrates were outgassed at approximately 400-500°C and maintained at that temperature during the run. Typical conditions for the deposition of several samples are listed in table 1. Table 2 presents a summary of data on one or two samples from each deposition run performed in this project.

TABLE 1

BORON NITRIDE DEPOSITION CONDITIONS

	BN47	BN48	BN55
Substrate Temperature (°C)	410	411	470
Nitrogen Pressure (torr)	8×10^{-5}	8×10^{-5}	8×10^{-5}
Filament Current (A)	8.0	~8.0	~8.0
Discharge Potential (V)	50	50	150
Discharge Current (mA)	230	200	200
Screen Accelerator Potential (kV)	0.30	0.25	0.35
Beam Potential (kV)	2.5	2.5	3.0
Ion Beam Current (μA) [substrate position]	10[A1]	14[A1]	30[A2]
Electron Beam Power (kW)	0.35	0.40	0.40
Deposition Time (hr)	3.0	3.0	3.0
Film Thickness on Si (μm) [substrate position]	2.7[C2]	2.4[B2]	3.6[B2]
Deposition Rate on Si (Å/min)	150	133	128

The ion beam distribution at the substrate plane changed and was rechecked each time the gun was removed for cleaning and maintenance. A typical distribution is given in figure 5. The values of the ion current listed in table 2 have been adjusted to represent the value for the specific substrate. The variability of the estimates of ion current may be high (perhaps ± 50%).

Table 2 also lists, in the last two columns, surface treatments and tensile bond strength measurements performed in the later work on adhesion, which is discussed in section 5.

TABLE 2

SUMMARY OF DEPOSITION CONDITIONS AND PROPERTIES OF SAMPLES

Sample	Substrate	N_2^+ Beam Current/Voltage ($\mu A/cm^2$/kV)	Thickness (μm)	Deposit Rate (Å/min)	Microhardness $\mu HV(5)$ (kg/mm^2)	Tensile Bond Strength (lbs/in^2)	Remarks
BN40-C2	SS 17-4	108/20	1.3	96		2,893	
BN41-B1	Si	150/20	1.2	50	3,122		
BN42-B1	Si	152/1.0	1.1	89	3,684		
-B2	SS 17-4	1070/1.0	1.1	89	3,622		
BN43-B1	Si	38/2.5	1.6	76			
BN44-C2	Si	7.0/2.5	2.7	128	3,073		
BN45-A2	Si	29/2.5	1.3	72	3,870		
BN46-B1	SS 440	30/2.5	2.7	140		2,716	
-B2	SS 440	180/2.5	3.7	192			
BN47-B2	SS 440	286/2.5	2.7	150			N_2^+ 1st
BN48-A2	Si	20/2.5	2.0	111	3,532		Boron 1st
-B2	SS 17-4	84/2.5	1.9	106		Peeled	
BN49-B2	Si	---	2.3	128	4,476		B only in N_2^+
BN50-C2	Si	25/2.5	3.1	172	2,190		
BN51-B2	SS 440	106/2.5	2.9	161		Peeled	Boron 1st
BN52-B2	SS 440	240/2.5	1.4	78			Etched
BN53-B2	SS 440	200/2.5	2.4	141		543	N_2^+ 1st
-A2	SS 440					2,806	
BN54-B2	SS 440	220/3.0	2.1	117		3,015	Boron 1st
-B3	SS 440	18/3.0	2.7	150	1,905	4,278	Boron 1st
BN55-B2	SS 17-4	600/3.0	3.6	200		6,722	B 1st, Electropol.
-C3	SS 17-4	491/3.0	3.0			3,169	Boron 1st
BN56-B2	SS 440	340/3.0	2.5	139		5,072	B 1st, Electropol.
-B3	SS 440	25/3.0	2.0			4,726	Boron 1st

	A	B	C
1	0.05	0.07	0.008
2	0.2	1.0	0.05
3	0.05	0.7	0.08

Front

Figure 5. Relative ion beam intensities at the nine substrate positions of the sample holder for depositions BN51 to BN56.

2.2 Deposition Procedure

The step by step procedure for coating production was as follows:

(1) Vacuum chamber was evacuated to the 10^{-6} torr range or below for several hours.

(2) Substrates were heated to 500°C for outgassing. Outgassing duration was one hour or longer.

(3) Both the ion gun filament and the electron beam filament were turned on during the outgassing procedure.

(4) When the pressure returned to its low value following the initial outgassing, the high voltage supply of the electron gun was activated and the boron was melted in the crucible in order to drive out residual gases.

(5) The ion gun and the electron gun filament were then turned off but the substrate heater remained on.

(6) Nitrogen gas was introduced into the ion gun by opening a needle valve and the pressure brought to 8×10^{-5} torr.

(7) The ion gun filament was turned on and its current raised to approximately 8 A.

(8) The discharge was initiated in the discharge chamber by raising the output of the separate discharge supply to about 100 volts.

(9) The shutter protecting the substrates was then opened, permitting the ion current to be read by the collector at the substrate position.

(10) The accelerator voltage and the beam voltage were then set.

(11) All power supplies were adjusted to maximize the ion current.

(12) The electron gun was turned on at an accelerating potential of 15 kV and its filament current slowly raised so that a pool of molten boron, surrounded by solid boron, formed in the water-cooled crucible. The boron evaporation rate was kept low enough to ensure an adequate ratio of nitrogen ions to boron atoms striking the substrate.

2.3 Substrate Motion Apparatus

The bearing components whose coating is contemplated are (a) an inner member whose surface is the portion of a sphere between parallel planes that divide the sphere's diameter approximately in thirds and (b) an outer member with a mating inner surface. To expose these bearing surfaces uniformly to the sources of boron atoms and nitrogen ions requires suitable orientation and rotation of the parts. Details of the requirements and the apparatus that was designed to meet them are given in appendix B.

3. INFRARED SPECTRA

Each deposition included a substrate of polished single crystal silicon, which was used for the determination of the BN structure by means of infrared analysis. A Bomem Michelson 110 Fourier Transform Infrared Spectrophotometer was used for this purpose. All of the infrared absorption spectra are shown in the appendix figures A1 to A16.

Three distinct absorption peaks (minima in the transmission curves) characterize the crystalline phase of the boron nitride films. The hexagonal phase exhibits a peak around 800 cm^{-1}, representing a B-N-B bending oscillation, and one around 1350 cm^{-1} representing a B-N stretching mode (figure A1). A single absorption band at approximately 1150 cm^{-1}, the fundamental transverse optical mode, is found for the cubic form (figures A2, A3). Samples of commercial cBN abrasives were prepared by mixing the powder with potassium bromide and pressing the mixture to a flat pellet. The 800 cm^{-1} peak also is present in the spectrum of the 60/80 mesh cBN abrasive but not in that of the 1.5-2 μm particle size sample. The spectra agree with those reported in the literature for boron nitride in bulk and in films[3,4].

The spectrum of pure vacuum-deposited boron is shown in figure A5. No strong absorption peaks of either the hexagonal or the cubic phase of BN appear in the spectrum of the boron sample.

Reflection interference bands are visible in all spectra of the thin films. The interference bands unfortunately distort the transmission curves so that the absorption band's relative strength is not immediately apparent. The absorption peak at around 600 cm^{-1} present in all samples arises from the silicon substrate (figure A5).

Figures A6 to A16 show spectra from boron nitride samples made by the ion-assisted thermal deposition process described in section 2. In general, absorption peaks characteristic of both hexagonal and cubic phases are present in the spectra of all samples.

4. MICROHARDNESS

The Vickers microhardness numbers of those samples which were measured are listed in table 2. These hardness numbers represent the actual contribution of the film rather than the hardness of the film-substrate composite, which is frequently what is reported [6]. The hardness of each sample was measured with a Reichert microhardness tester by using its Vickers diamond indenter to make a series of indentations at increasing loads on the sample surface. A scanning electron microscope was used to measure the diagonal of each indentation. The data were then plotted in a log-log graph of load versus diagonal (the Meyer plot). A typical plot of such data is shown in figure 6. The log-log plots usually show two straight-line segments. The line established by the smaller indentations, at the lower loads, represents the hardness of the coating, while the line formed at higher loads represents the coating plus the substrate. The lower-load line was used to determine the microhardness according to the following procedure:

(1) The parameters n and a of the equation for the Meyer line

$$L = ad^n, \qquad (1)$$

where L = indenter load

and d = diagonal width of the indentation

are determined by a least-squares fit of a straight line to the points on the log-log plot that lie below a load value selected by inspection of the graph; and

(2) the microhardness μHV(L) of the film at a particular load L is calculated by the relation:

$$\mu HV(L) = 1854.4L^{(1-2/n)}a^{2/n} \qquad (2)$$

where μHV is in kilograms force per square millimeter, L is in grams force, and d is in micrometers.

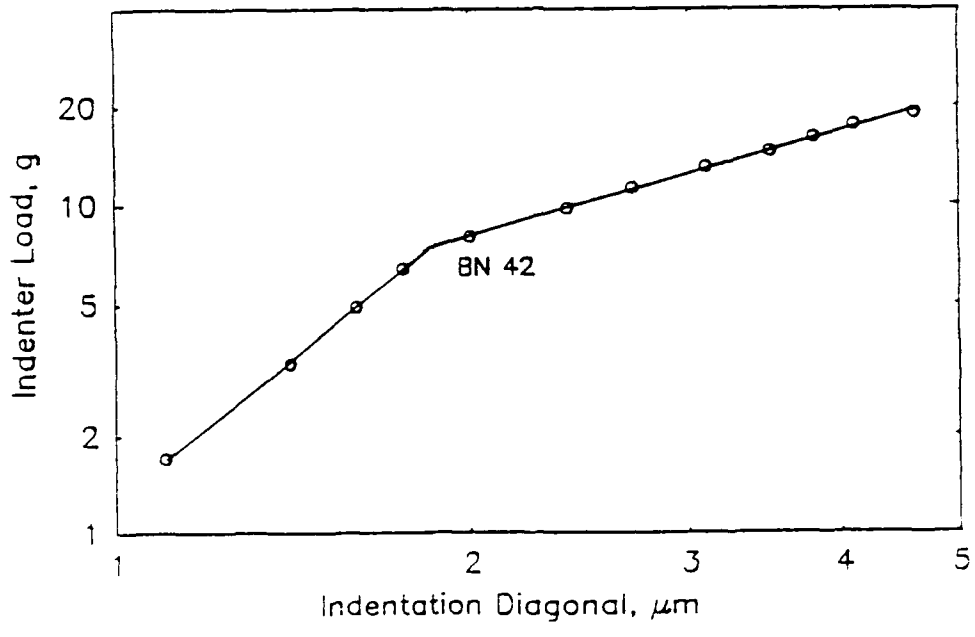

Figure 6. Meyer plot for sample BN42-B2.

When the coefficient n differs from 2, the microhardness values μHV(L) are different at different loads L. A load of 5 gf was selected for calculating the μHV values in table 2. Microhardness value for typical samples at 5 and 10 gf, as well as the Meyer line parameters, are given in table 3. Hardnesses were frequently measured on the silicon substrate rather than the stainless steel substrates so that the hardness could be directly correlated with the infrared spectrum. Microhardness values in the 3000-4000 kg/mm^2 range are considered to represent a good hard coating, inasmuch as the microhardness of titanium nitride coatings at a 10-gf load is about 2000 kg/mm^2[7]. Unfortunately, the Meyer curve parameters were not quoted in the report on titanium nitride and it is therefore difficult to compare values. The hardness of BN48-A2 at a 10-gf load, for example, is 4275 kg/mm^2.

TABLE 3

VICKERS MICROHARDNESS OF BN COATINGS

$$\mu HV \text{ (load in grams)} = 1854.4L^{(1-2/n)}\, a^{(2/n)}$$

Sample	Substrate	Thickness (μm)	a	n	μHV(5) (kg/mm^2)	μHV(10) (kg/mm^2)
BN42-B2	17-4 SS	2.0	1.28	2.85	3622	4391
BN44-C2	Silicon	2.7	1.82	1.83	3073	2881
BN48-A2	Silicon	2.0	2.76	1.32	3532	4275
BN49-B2	Silicon	2.3	1.50	2.90	4476	3544

The ratio of the peak heights in the infrared spectra (section 3) is related to the ratio of hexagonal to cubic phase within each sample. Although that ratio varies, table 2 shows that all samples exhibit high microhardness. Although the data do not show conclusively that samples containing a larger proportion of the cubic phase exhibit higher hardness values, there does appear to be a tendency in that direction. Sample BN42, for example, has more cubic phase than BN41, and is slightly harder (3684 kg/mm^2 vs. 3122 kg/mm^2). The film with the highest microhardness value, BN49 (table 2), shows the 1150 cm^{-1} cubic peak as well as structure at 800 cm^{-1}. One of the hardest films, represented by sample BN45-A2, shows strong absorption bands characteristic of the hexagonal phase only. Sample BN44 exhibits no peak characteristic of hexagonal form, but its microhardness is low. These results are in agreement with the findings of other workers - the hardness of the films appears to be somewhat insensitive to the relative proportions of hexagonal and cubic form[3] - but in disagreement with reference [4].

5. ADHESION

During the early part of this study, the films were tested for adhesion with the Scotch tape specified by ANSI/ASTM Standard D 3359-78 and none of the coating came off. Immersion several times in liquid nitrogen of a sample deposited on stainless steel left the coating unaffected. Although the cycling between approximately 25° and -196°C does not represent expected environmental exposures, the rate of temperature change was believed to be higher than would occur in practical bearings. It appeared from these preliminary tests that thermal shock and differences in thermal expansion would not affect the adhesion of the coating.

The following samples were delivered to MTL in September 1989:

Sample No.	Type of Steel	Coating Thickness micrometers
BN42-B2	17-4	2
BN46-B2	440	3.7
BN47-B1	17-4	1.6
BN47-B2	440	2.7
BN48-B2	17-4	2.4

Scratch adhesion tests were performed subsequently at MTL by Prof. Theo Z. Kattamis, Department of Metallurgy, University of Connecticut. Prof. Kattamis is evaluating tribological properties of coatings at MTL under the Army's Scientific Services Program. Details of the test apparatus, procedures, and results are given in Appendix C. Adhesion and cohesion data supported by metallographic observations showed that the coatings were weak and adhered poorly to the stainless steel substrates compared with hard coatings deposited by several other methods.

When the results of the scratch tests performed at MTL became known, tensile bond strength tests were initiated and efforts were made to modify the interface between the film and substrate for improved adhesion.

5.1 Tensile Bond Strength Tests

A standard tension test for adhesive bond strength (ASTM D 2095) was modified for testing the thin coatings on one-inch square substrates. Small rods, usually aluminum, 1/4 or 3/8 in. in diameter with ends machined flat, were cemented to the surface of the coating with 3M ScotchWeld structural adhesive no. 22144 NMF. Prior tests with this adhesive indicated that it has a tensile strength of 9,000 to 10,000 lb/in^2. The adhesive is a two-part epoxy mixture

and requires curing at 200°-250°F. A drop of freshly mixed adhesive was applied to the carefully cleaned end of the rod and the rod was set on the film and pressed into close contact. Then the specimen was left undisturbed in an oven at 200°-210°F for at least 3-4 hours, generally over night. Tests of the films were generally carried out a day after the adhesive was set. The specimen was mounted in an Instron testing machine by clamping the rod in conventional testing grips and clamping the square metal substrate in a machinist's vise held on the Instron crosshead with a C-clamp. Positioning and clamping was done carefully by eye so that the axis of the testing machine was parallel to that of the rod and the bending moment was minimized. The crosshead was lowered at a rate of either 0.002 or 0.005 in. per minute and the force was recorded at a chart speed of 0.5 in./min. The slow speed was used to ensure that the instrumentation could follow the behavior of the specimen even though its elastic deformation was very small.

During the test, the recorder chart showed a rising force until the film and/or the adhesive failed, at which point there was an abrupt drop in the force. A typical chart recording is shown in figure 7.

5.2 Substrate Surface Modifications

The following methods of surface modification were tested for improvement of the coating adhesion:

(1) Bombardment of the surface with N_2^+ ions prior to deposition;

(2) Deposition of a thin layer of boron at low pressure on the substrate prior to the introduction of nitrogen and the startup of the ion beam;

(3) Mechanical polish followed by chemical etching;

(4) Mechanical polish followed by electropolishing in acid (e.g., 70% nitric + 30% acetic).

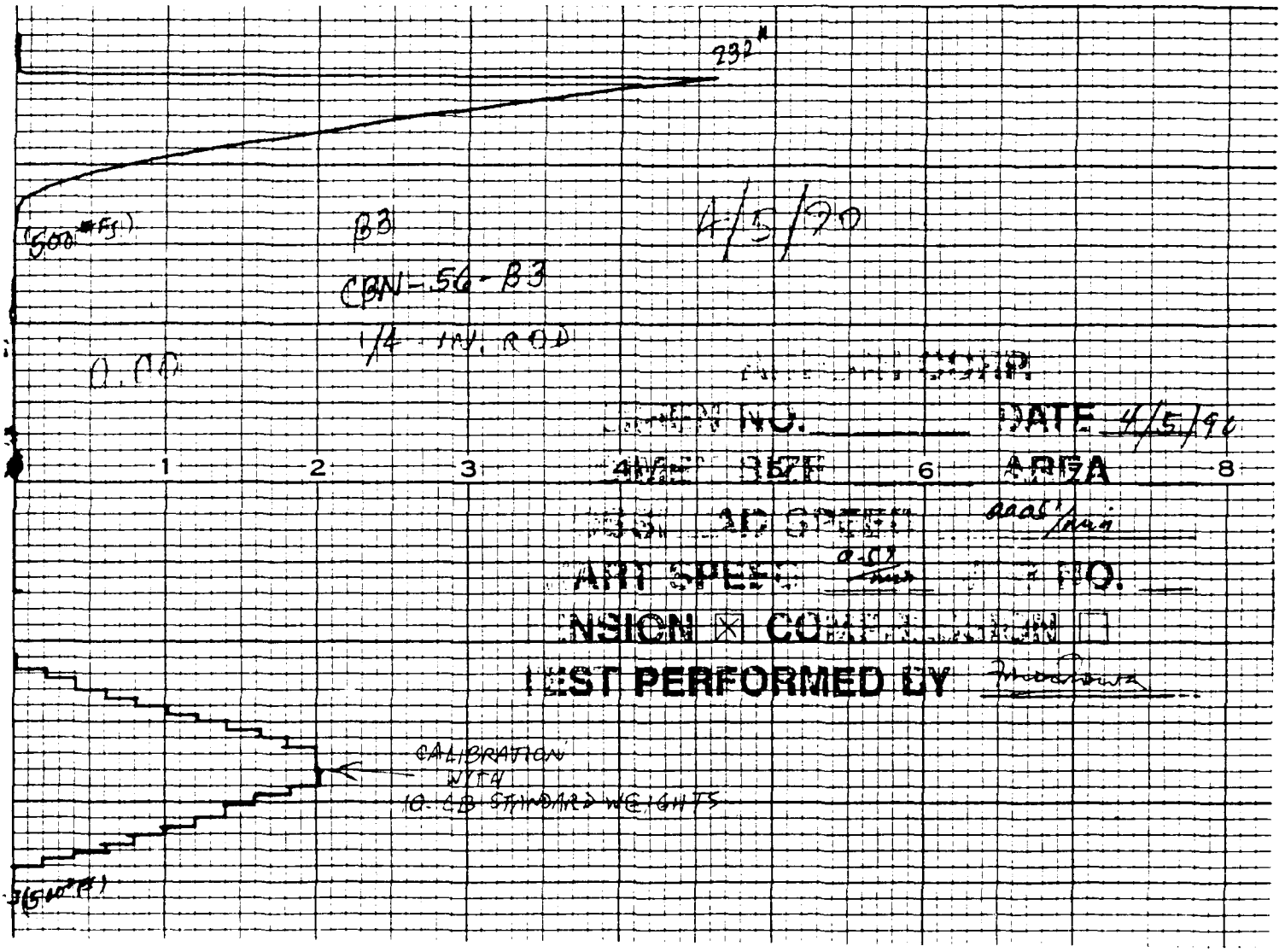

Figure 7. Recorder chart from tensile bond strength test of BN56-B3, showing scale calibration with ten standard 10-lb weights and tension test to a load of 232 lb force at failure.

5.3 Test Results

The results of the bond strength tests are given in table 4. Samples BN46-B1 and BN48-B1 were companions to those delivered to MTL for scratch adhesion tests. Sample films BN48-B1 and BN45-C2 adhered so poorly that the tension test could not be completed, while BN46-B1 adhered well.

TABLE 4

TENSILE BOND STRENGTH TESTS*
OF BORON NITRIDE FILMS

Sample	Substrate	Rod Diameter in. and (Material)	Force At Failure lb	Calculated Bond Strength $lb/in.^2$
BN40-C2	SS 17-4	1/4 (Al)	142	2893
BN46-B1	SS 440	3/8 (Al)	300	2716
BN48-B2	SS 17-4	3/8 (Al)	Failed	--
BN53-B2	SS 440	3/8 (Al)	60	543
BN53-A2	SS 440	3/8 (Al)	310	2806
BN54-B3	SS 440	1/4 (SS)	210	4278
BN54-B2	SS 440	1/4 (SS)	148	3015
BN55-C3	SS (?)	3/8 (Al)	350	3169
BN55-B2	SS 17-4 (Electropolished)	1/4 (Al)	330	6722
BN56-B2	SS 440 (Electropolished)	3/8 (Al)	560	5072
BN56-B3	SS 440	1/4 (Al)	231	4726

* Crosshead speed 0.005 in./min and chart speed 0.5 in./min.

The calculated tensile strength, based on the cross-sectional area of the rod, actually represents a lower limit, inasmuch as the bond between film and substrate usually fails only over a fraction of the cemented area. In some tests, this fraction was only 10-30%. A photograph of the two fracture surfaces of a typical sample is shown in figure 8.

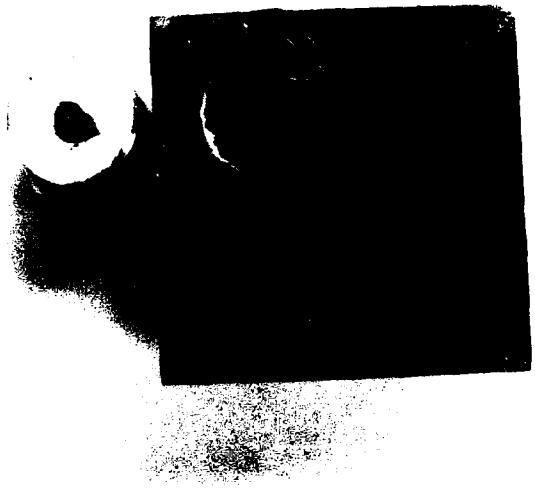

Figure 8. Fracture surfaces after bond strength test of sample BN56-B2. The area of the coating detached from the substrate, relative to the cross section of the rod, indicates the degree to which the test result may underestimate the bond strength.

The highest bond strength achieved was on a substrate that was electropolished first, followed by a boron coating prior to boron nitride deposition. The value of 6722 kg/cm^2 for BN55-B2 indicates that relatively good adhesion can be achieved for these films. Cutting and polishing of the coupons apparently leaves residues on the surface that must be removed chemically. Since boron forms compounds with most of the elements in the stainless steel (e.g., CrB_2, FeB) the initial layer of pure boron could form a strong chemical bond to a clean, well-outgassed surface at 400-500°C. Bombardment with N_2^+ ions did not appear helpful; instead, it may prevent the formation of the metal borides.

5.4 Subsequent Observations

Three to four months after completion of the experimental work, the samples subjected to the bond strength test were inspected in preparation for shipment to MTL. It was found that most of the film area in the samples showing the highest bond strengths had cracked in a fine pattern and largely spalled off in fragments ranging from about 0.05 to 0.5 mm in size. It had been expected that the BN films would be under compression in view of the difference in thermal expansion coefficient between cBN and steel; in fact, that may have contributed to high microhardness values. The cause of the delayed delamination is not clear. The earlier samples showing lower bond strength did not spall. Reaction of traces of oxides with atmospheric moisture in high summer humidity may provide a chemical explanation of the phenomenon, or crack growth along the brittle interface may propagate from initial edges and imperfections by the purely physical process well known in fracture mechanics. It remains to be determined whether the usual approach to this difficulty - reducing the film thickness to reduce the interfacial shear stress - can ameliorate the effect. The fact that boron coatings were made and studied by the author for years without observing such a reaction suggests that it should be avoidable with boron nitride.

6. CONCLUSIONS

The data presented in table 2 show that boron nitride films with both high hardness and high adhesion can be achieved on stainless steel substrates. One of the hardest coatings, containing primarily the cubic phase, was a boron film evaporated in a nitrogen environment without ion bombardment (BN49). High initial bond strength was obtained by depositing a layer of pure boron at low pressure prior to the introduction of nitrogen. Bombarding the sample surface with nitrogen prior to deposition did not result in high adhesion. Nitrogen adsorbed on the surface may have prevented compound formation between boron and the substrate constituents.

The poor performance of the samples delivered to MTL in the subsequent scratch tests described in appendix C and the delayed onset of spalling discussed in section 5.4 demonstrates that the coatings produced during this program would not be satisfactory in the bearing application. Since the mechanism of deterioration has not been established, the scratch test results and observations of spalling cannot be correlated with the measurements of hardness made comparatively soon after deposition.

It is clear that further work is required to improve the long-term stability of the cBN coating, followed by establishment of conditions for optimum hardness and adhesion and demonstration of performance on actual bearing components, to obtain the benefits of mechanical and chemical stability offered by cubic boron nitride for bearings and for many other applications required by the nation's future military and industrial equipment.

7. REFERENCES

[1] F. Ordway and C. Feldman, "Hard Coatings for Optical Surfaces", Final Report, Contract No. DAAL04-86-C-0005, ARTECH report J8637-FR (1987).

[2] K. Miyoshi, D. H. Buckley, and T. Syalvins, "Tribological Properties of Boron Nitride Synthesized by Ion Beam Deposition", J. Vac. Sci. Technol. A3, 2340 (1985).

[3] Y. Andoh, K. Ogata, Y. Suzuki, E. Kamito, M. Satou, and F. Fujimoto, "Properties of Boron Nitride Coating Films Prepared by the Ion Beam and Vapor Deposition Method (IVD)", Nuclear Instruments and Methods in Physics Research, B19/20, 787 (1987).

[4] K. Inagawa, K. Watanabe, H. Ohsone, K. Saitoh, and A. Itoh, "Preparation of Cubic Boron Nitride Film by Activated Reactive Evaporation with a Gas Activation Nozzle", J. Vac. Sci. Technol. A5, 2696 (1987).

[5] J. C. Angus, J. E. Stultz, P. J. Shiller, J. R. MacDonald, M. J. Mirtich, and S. Domitz, "Composition and Preparation of the So-Called Diamond-Like Amorphous Carbon Films", Thin Solid Films, 118, 311 (1984).

[6] C. Feldman, F. Ordway, and J. Bernstein, "Distinguishing Thin Film and Substrate Contributions in Microindentation Hardness Measurements", J. Vac. Sci. Technol. A8, 117 (1990).

[7] J. E. Sundgren and H. T. G. Hentzell, "A Review of the Present State of Art in Hard Coatings Grown From the Vapor Phase", J. Vac. Sci. Technol. A21, 2259 (1086).

APPENDIX

A. Infrared Spectra

B. Motion Apparatus for Coating Bearing Components

C. Evaluation of the Friction Coefficient of Boron Nitride Coatings and their Adhesion to 440 or PH 17-4 Stainless Steel Substrates (by Prof. Theo Z. Kattamis)

APPENDIX A

Infrared Spectra

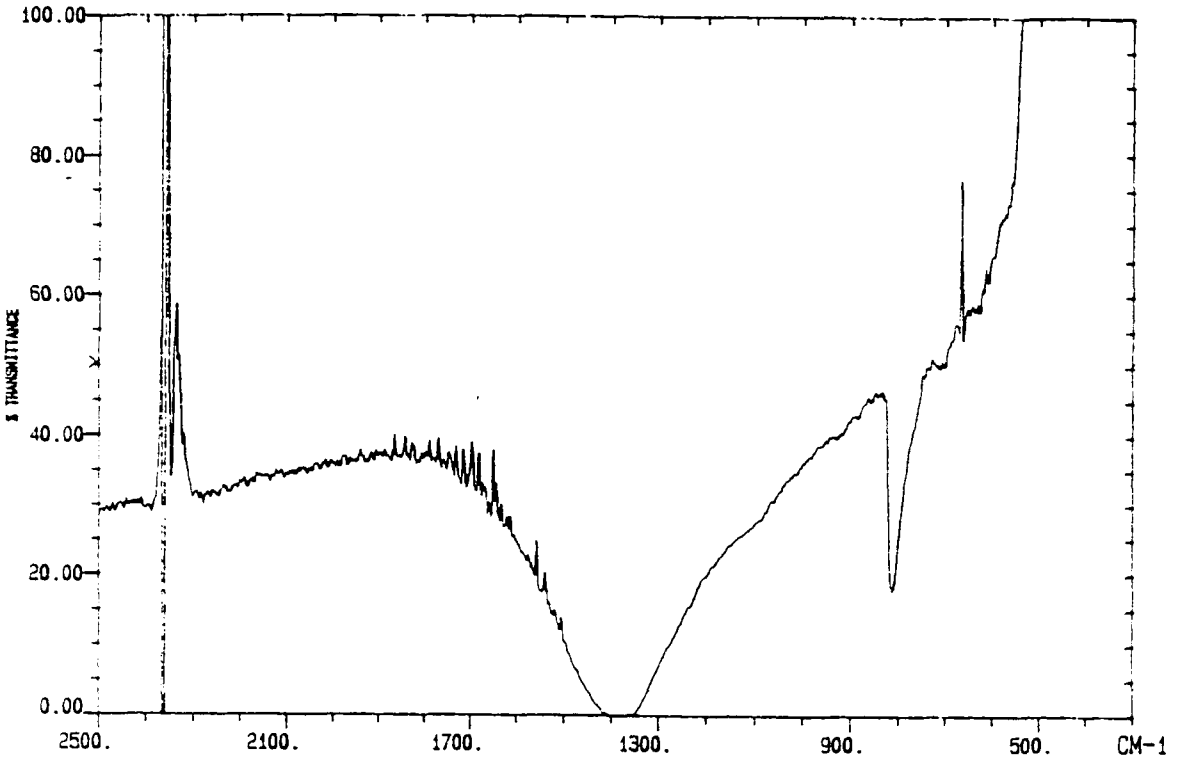

Figure A1. Infrared spectrum of Carborundum hexagonal boron nitride.

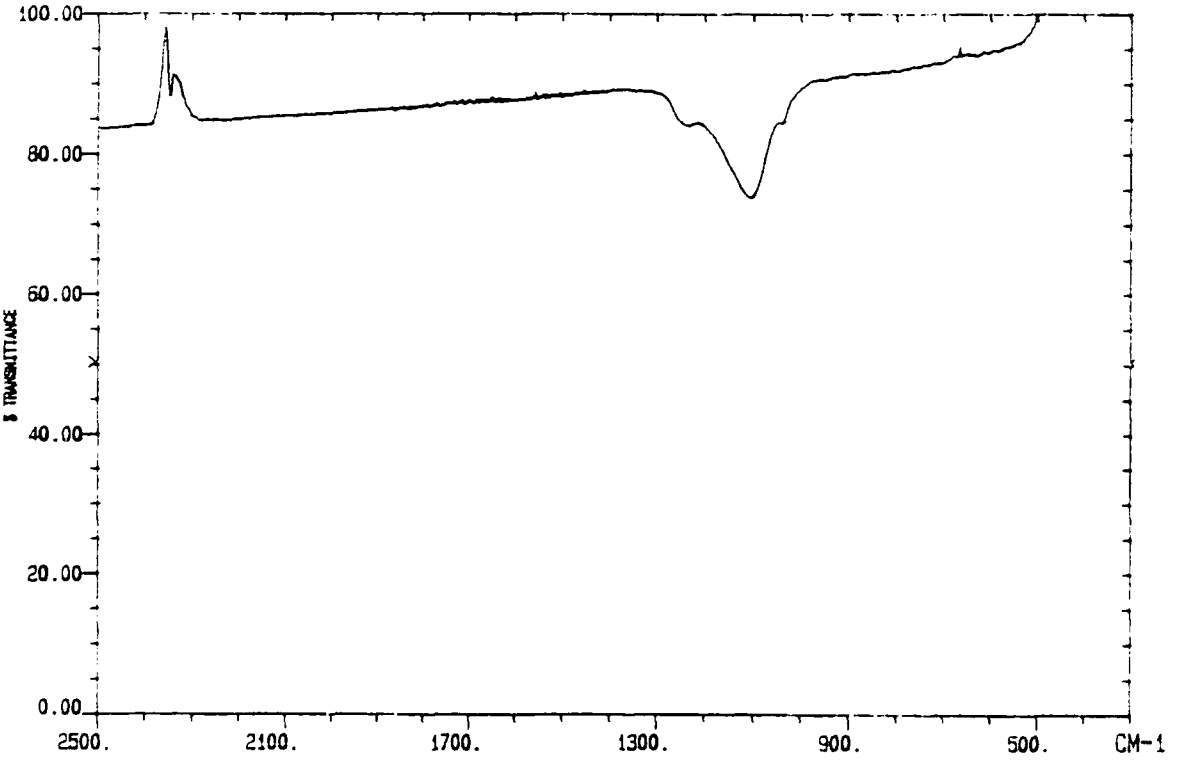

Figure A2. Infrared spectrum of General Electric cubic boron nitride, 1-1/2 - 2 micron particle size.

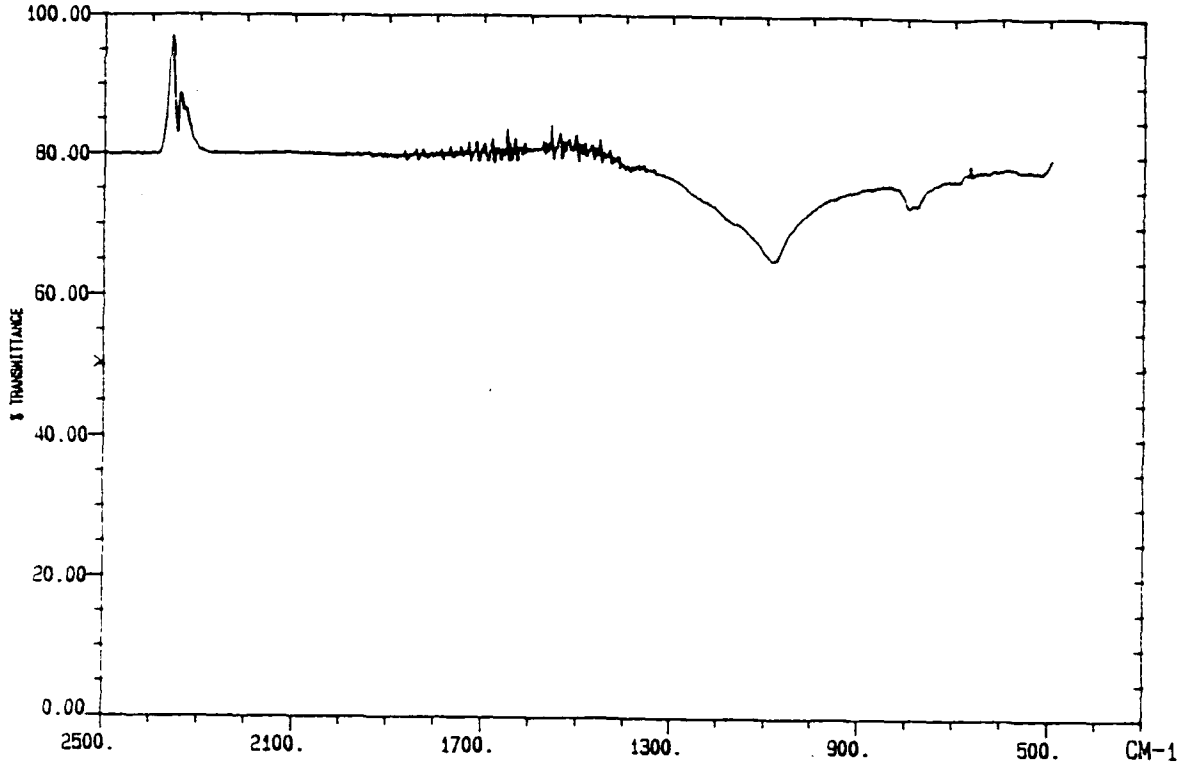

Figure A3. Infrared spectrum of General Electric cubic boron nitride, 60-80 mesh particle size.

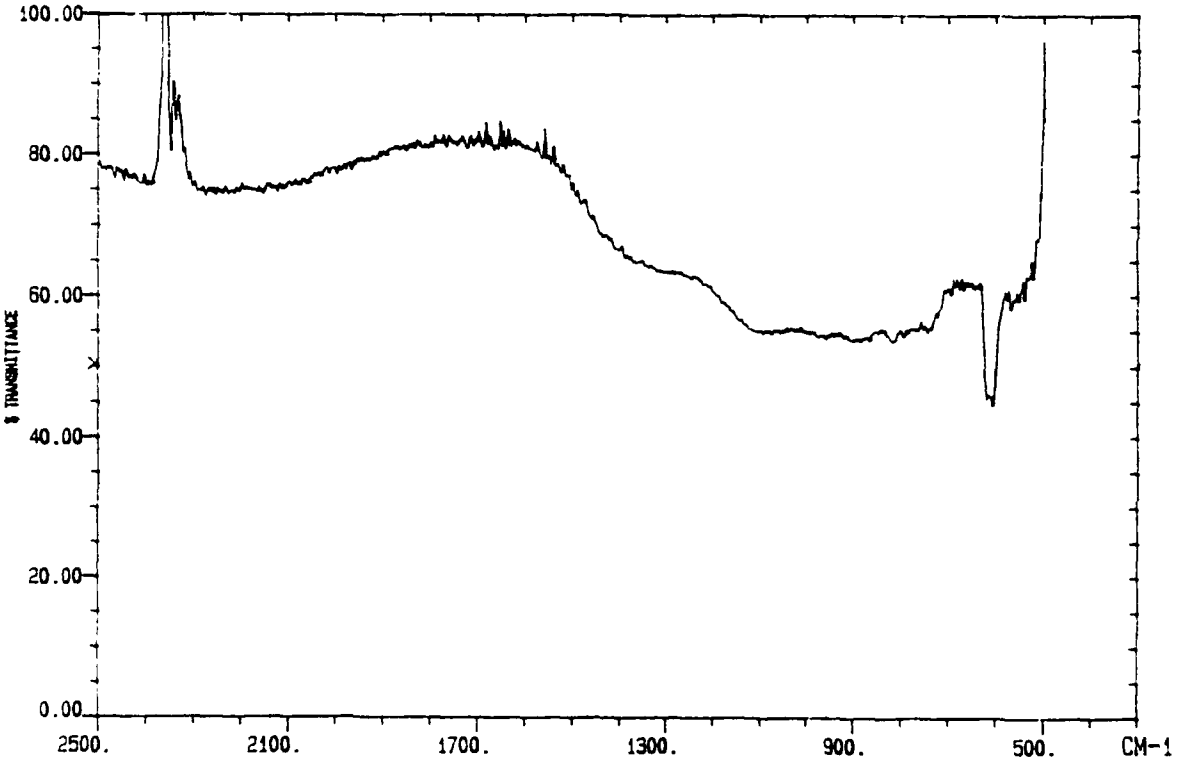

Figure A4. Infrared spectrum of sample BN35-B2 (pure boron film).

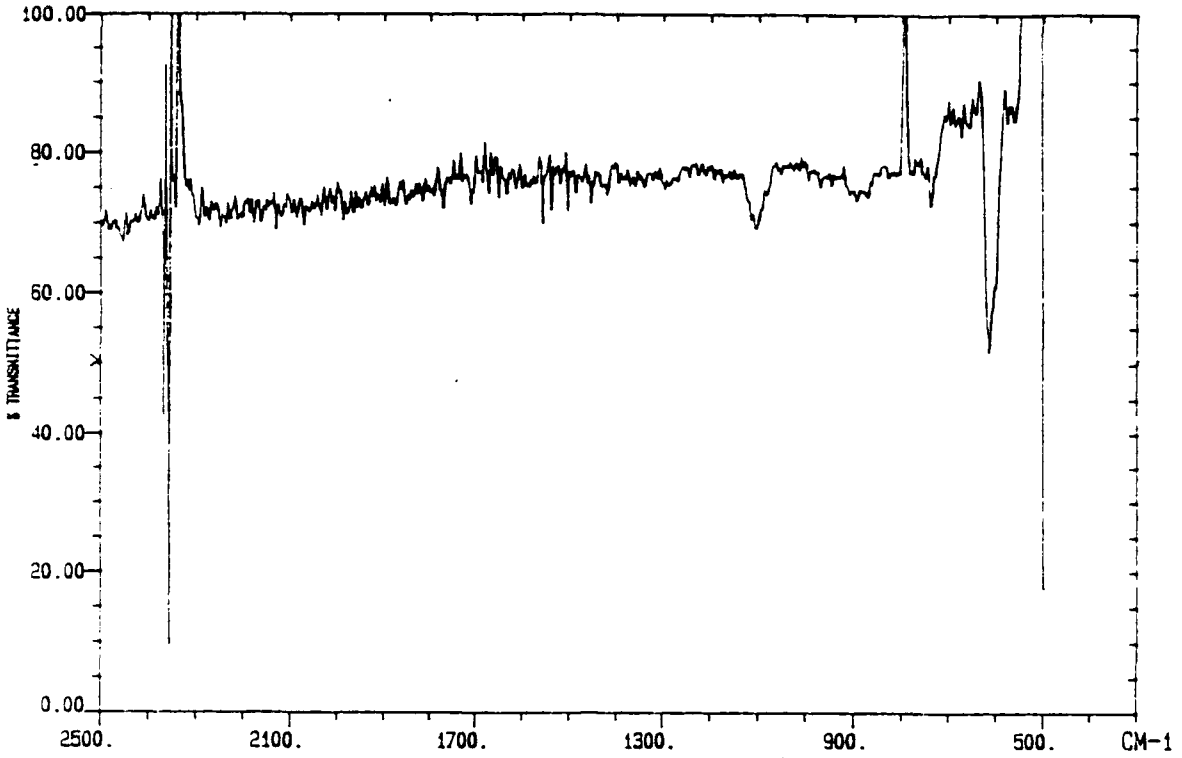

Figure A5. Infrared spectrum of uncoated silicon wafer.

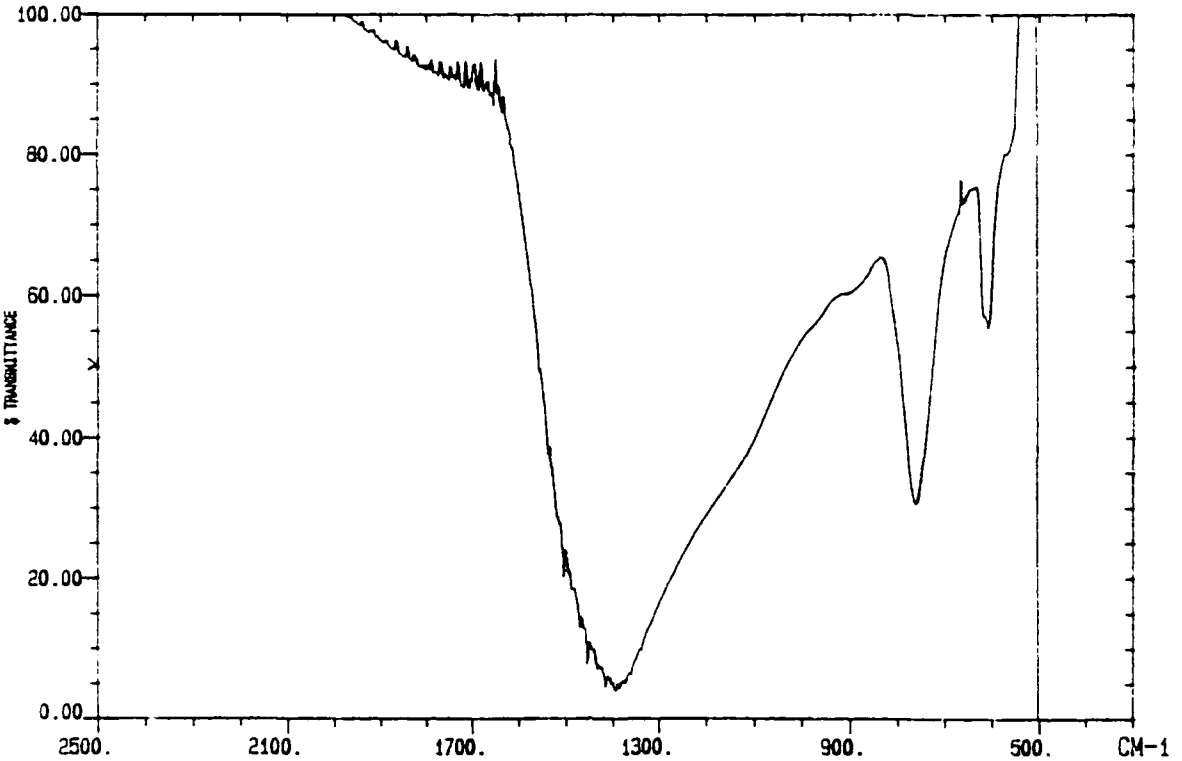

Figure A6. Infrared spectrum of sample BN41-B1.

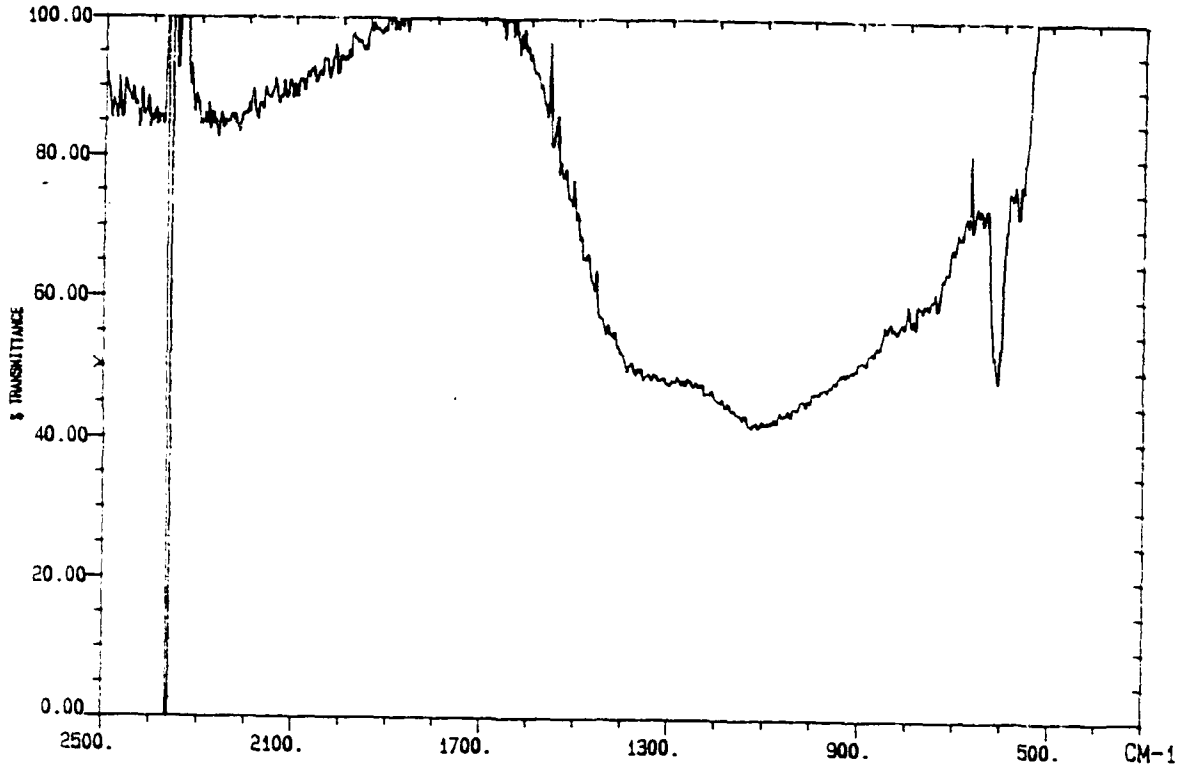

Figure A7. Infrared spectrum of sample BN42-B1.

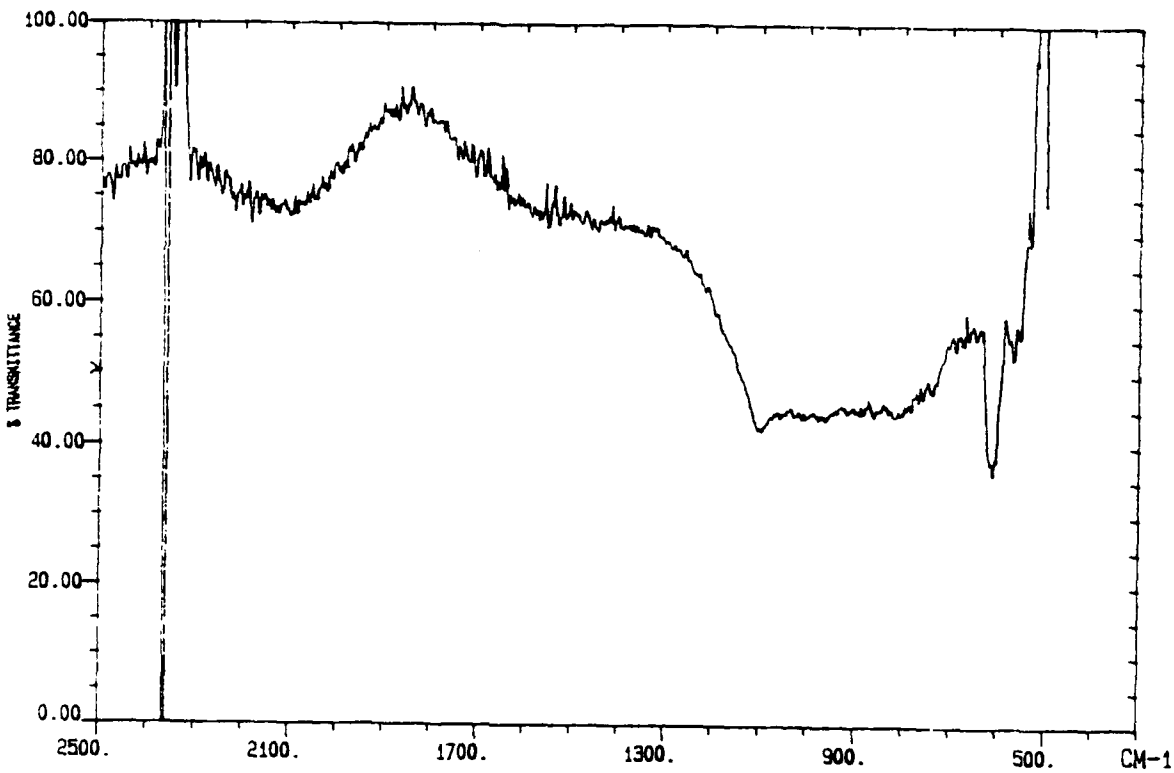

Figure A8. Infrared spectrum of sample BN44-B3.

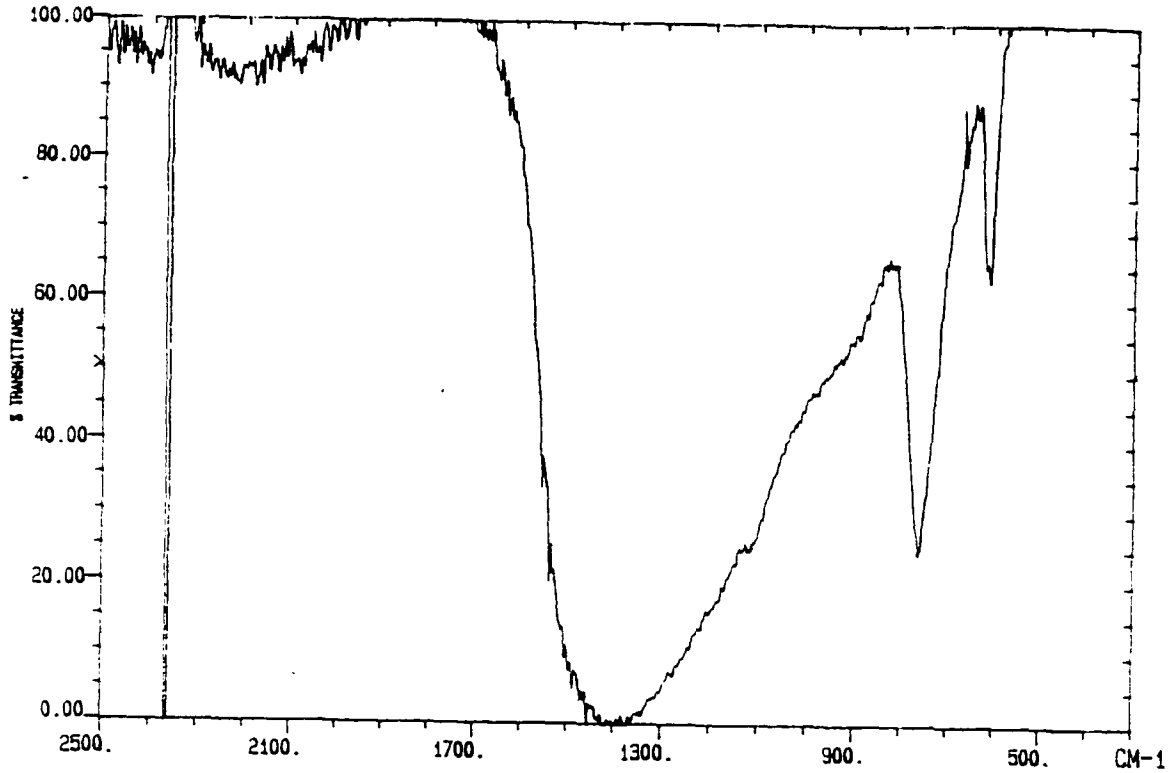

Figure A9. Infrared spectrum of sample BN45-A2.

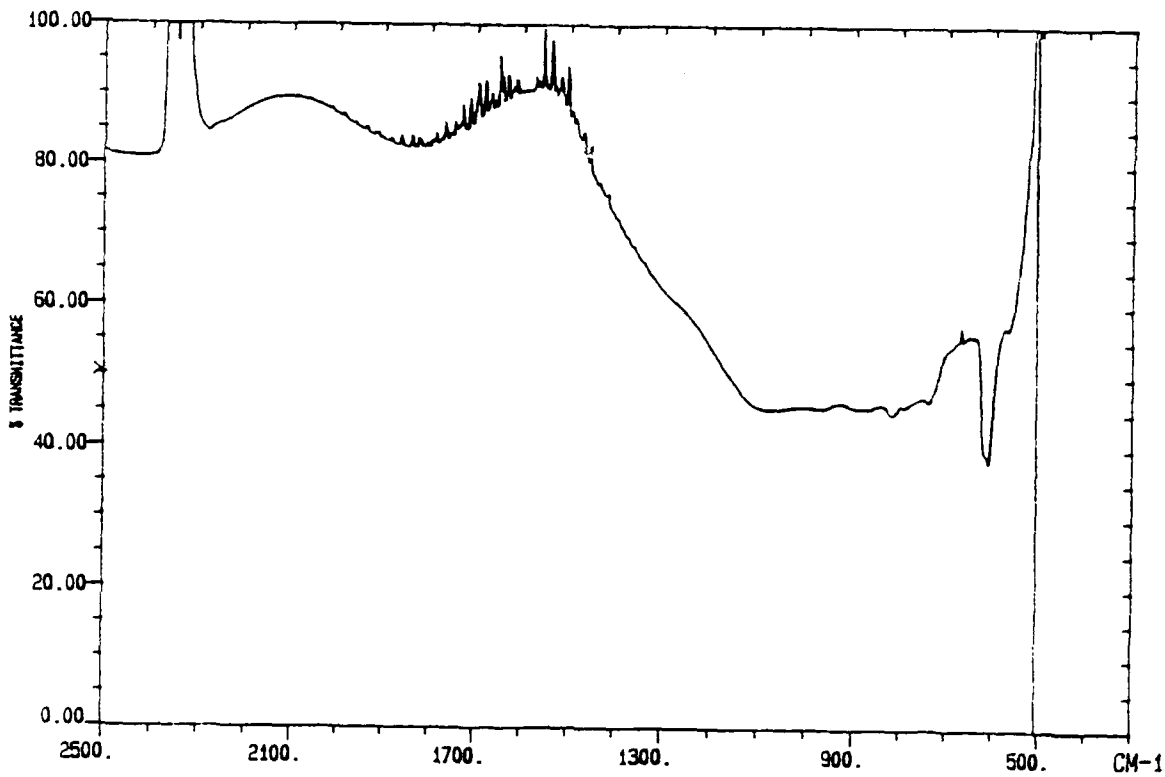

Figure A10. Infrared spectrum of sample BN47-C2.

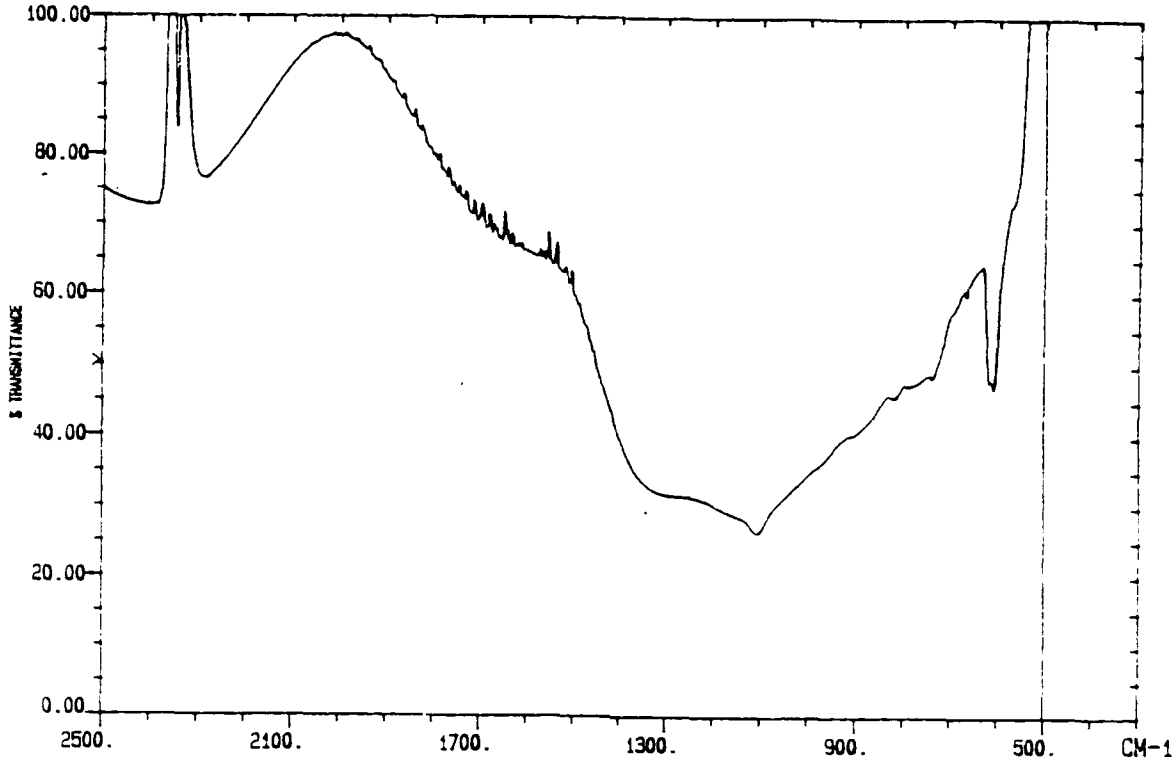

Figure A11. Infrared spectrum of sample BN48-A2.

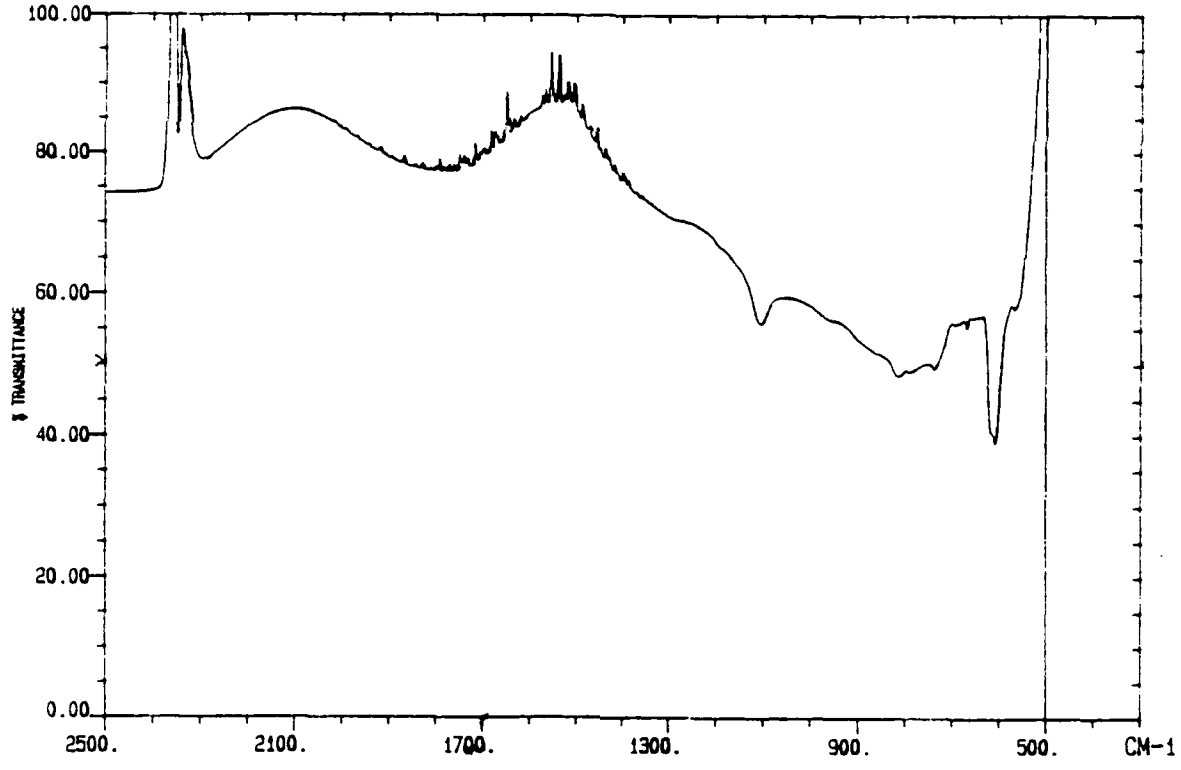

Figure A12. Infrared spectrum of sample BN49-32.

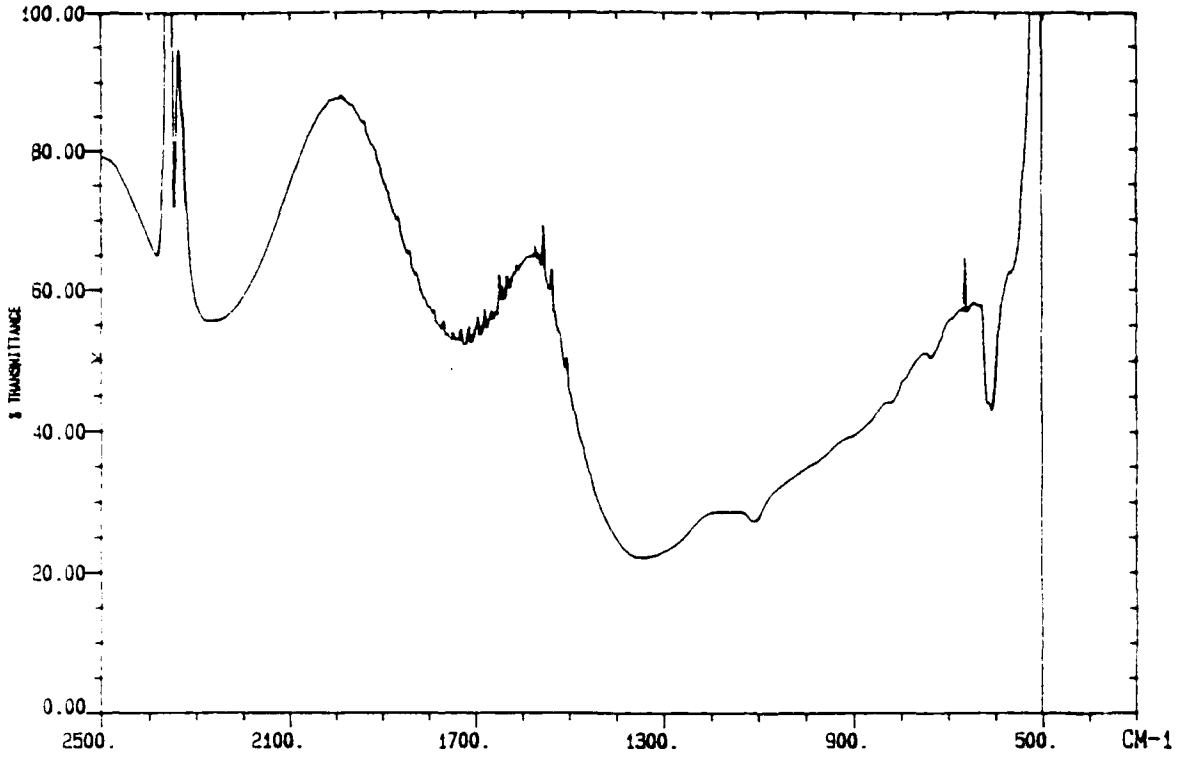

Figure A13. Infrared spectrum of sample BN50-C2.

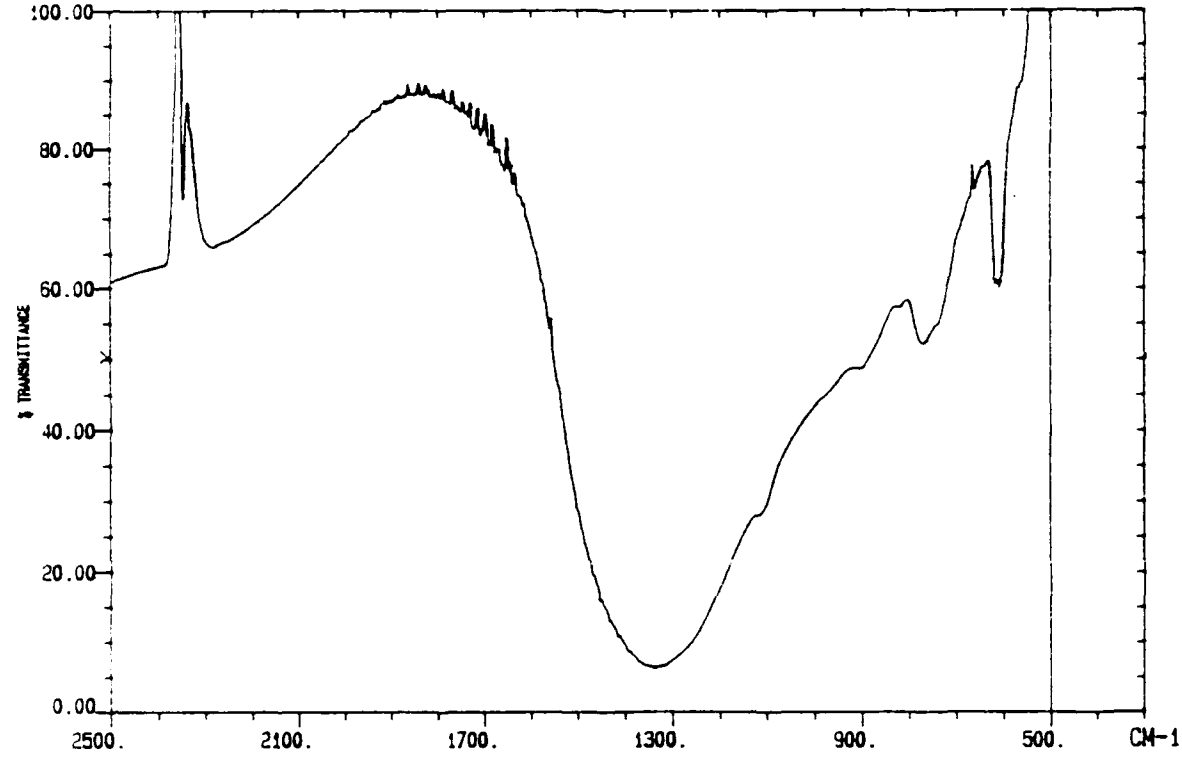

Figure A14. Infrared spectrum of sample BN54-A2.

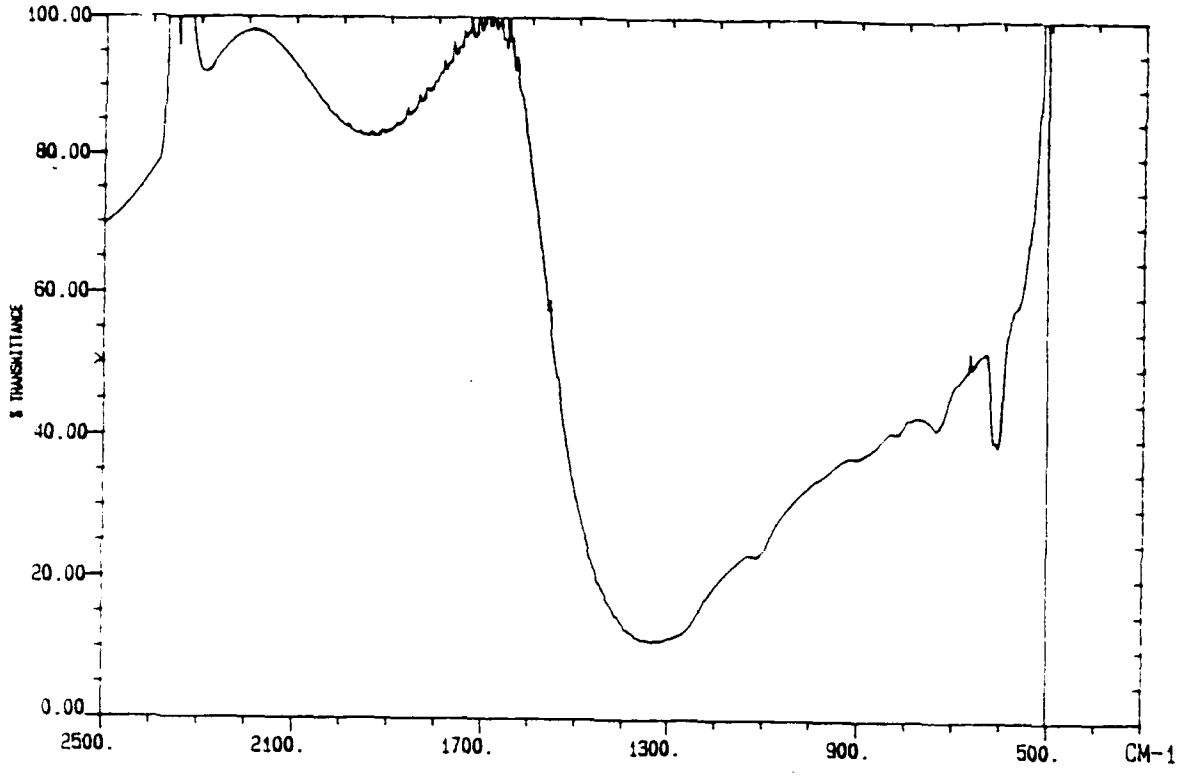

Figure A15. Infrared spectrum of sample BN55-A3.

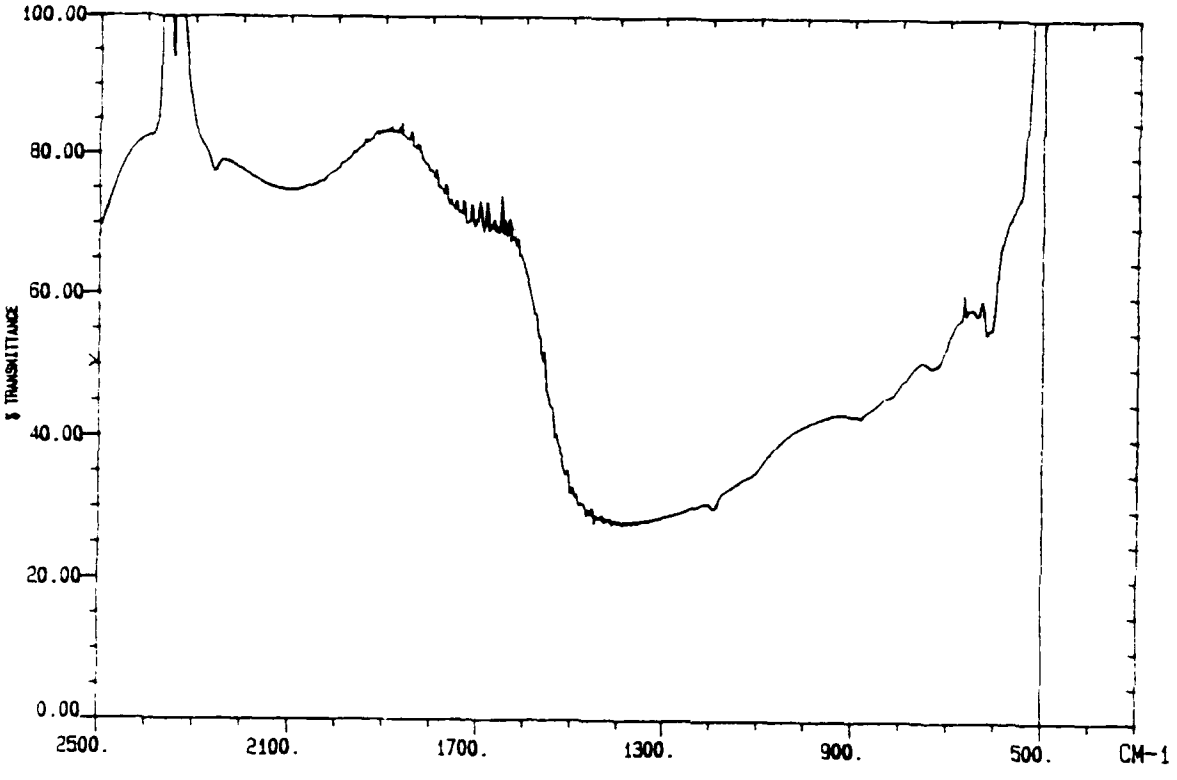

Figure A16. Infrared spectrum of sample BN56-C3.

APPENDIX B

Motion Apparatus for Coating Bearing Components

B. MOTION APPARATUS FOR COATING BEARING COMPONENTS

B.1 Required Performance Features

The design of the rotating/tilting sample holder was required to embody the following performance features:

(1) All stainless steel construction free of potentially volatile metals, plastics, etc.;

(2) Free from lubricants and other contaminants;

(3) Free from trapped voids that could act as virtual leaks (e.g., fastened with screws that are drilled axially for evacuation of the holes they fit in);

(4) Rotates the inside/outside bearing components (size range up to that of an ordinary doughnut) at a speed in the range 1-60 rpm;

(5) Grips the inside/outside bearing component on its inner/outer surface with negligible shadowing of the deposited film;

(6) Capable of tilting the axis of sample rotation from horizontal by 0 to $\pm$ 30°;

(7) Has the axis of tilt passing through the geometric center of the rotating sample;

(8) Changes the tilt angle either by (a) oscillating 1-60 times per hour over a prescribed range or (b) cyclically alternating between two prescribed tilts with a prescribed dwell time of 10-300 seconds between angle changes requiring less than 10 seconds.

B.2 Mechanical Design

The design meets the foregoing requirements as follows.

All materials are stainless steel, unlubricated except by solid films acceptable in high vacuum systems. All threaded fasteners are vented. Thus requirements (1)-(3) are met.

The requirement for independent rotation and tilt motions is met by the installation of two rotary feedthroughs on the vacuum chamber accessory collar. One is driven by a continuous-rotation adjustable-speed motor and controller mentioned above and the other is driven by a stepping motor with appropriate step control circuitry.

The sample holder shaft is supported by a plate that is basically C-shaped, with the bearing component in the opening of the C so that the plate can be supported on two pivots whose axis passes through the center of the bearing component. The tilt adjustment is controlled by rotation of a threaded vertical shaft driven by the stepper-actuated feedthrough through a pair of bevel gears.

The continuous motion feedthrough, through a chain and sprocket linkage, drives a shaft mounted on the tilting place coaxially with the tilt pivots; thus the sample rotation can be maintained in spite of changes in tilt of the sample holder shaft. The shaft along the tilt axis drives the sample holder shaft through two auxiliary shafts, providing three 90° changes in the direction of the axis of rotation through three sets of level gears. Ultimately the last axis of rotation, that of the sample holder shaft, is fixed at right angles to the shaft along the tilt axis, but the plane in which they lie can rotate $\pm 30°$ from the horizontal.

By this mechanism, requirements (4)-(7) are met.

B.3 Controls

The adjustable-speed motor is driven by a solid-state circuit with a feedback controller, which holds the speed constant by measuring the back-e.m.f. of the motor.

The stepping motor is controlled by a TRS-80 Model III computer, whose program provides for rotation through any desired angle at a predetermined speed in performance of any desired program or cycle as indicated in requirement (8).

APPENDIX C

Evaluation of the Friction Coefficient of Boron Nitride Coatings and Their Adhesion to 440 or PH 17-4 Stainless Steel Substrates

(by Prof. Theo Z. Kattamis)

EVALUATION OF THE FRICTION COEFFICIENT OF BORON NITRIDE COATINGS AND THEIR ADHESION TO 440 OR PH 17-4 STAINLESS STEEL SUBSTRATES

Theo Z. Kattamis
Department of Metallurgy
University of Connecticut
Storrs, CT 06268

For ARMY MATERIALS TECHNOLOGY LABORATORY

The friction coefficient or, in fact, the scratching coedfficient, the cohesive load at which crack initiation occurs within the coating, and the adhesive load at which the crack propagates at the coating-substrate interface causing delamination were evaluated with a CSEM-Revetest automatic scratch testing apparatus, Fig.1, coupled with an X-Y chart recorder. The apparatus includes a diamond indenter with an original tip radius of 0.2mm, a load cell, a load driving motor, a sample table with a driving motor and a screw drive for manual sample stage displacement. Two proximity switches limit the end of the stroke of the sample table and two others limit the end of the stroke of the loading device. This apparatus includes also a resonant acoustic emission detector with an acoustic emission preamplifier, amplifier and signal converter.

The testing procedure may be summarized as follows: The diamond point first comes down until it touches the surface of the sample. Then the normal load, F_n, applied to the diamond stylus immediately starts to increase linearly with time and its instantaneous value is displayed. When this force exceeds the preselected lower load the sample starts to move at constant velocity and continues until the applied force reaches the desired upper limit load. The diamond is then lifted-up from the sample surface and the table moves back automatically to its original position, so after lateral translation the equipment is ready for the next test. Under these linearly variable normal load conditions the scratch testing apparatus provides the frictional or tangential force, the friction coefficient and the acoustic emission signal intensity versus normal load between preset limits. In a different operating mode scratch testing is possible under constant normal load conditions and for a very low load provides the usual friction coefficient.

Five BN-coated 440 and PH 17-4 stainless steel specimens processed by ARCTECH were evaluated with the scratch tester, as well as metallographically. Results are as follows:

BN 47
B2
SS 440

The Acoustic Emission (AE) signal intensity and the scratching coefficient (μ^*) are plotted in Fig. 2 versus normal load between 0 and 70N. Photomicrographs of the scratch are exhibited in Fig. 3. Plastic deformation of the coating is observed up to a load of 6.29N at which the first microcrack appears at the edges of the scratch. With increasing load the first transverse microcracks appear within the track at a load of about 7.80N and the first signs of delamination within the track at 7.90N, Figs. 3a and f. Well developed primary transverse microcracks accompanied by

secondary microcracks appear at 9.63N. The coating has been completely removed from the track at 14.81N. At 19.27N a dense network of microcracks appears within the denuded substrate in the track together with longitudinal striations by the edges of the scratch. Beyond a load of 54.36N the transverse microcracks become wider and their spacing larger.

Fig. 2 shows that the cohesive load L_C=6.29N (corresponding to crack initiation within the coating), is attained at 0.616mm from the beginning of the scratch, whereas the adhesive load L_A=8.05N (corresponding to crack propagation at the coating-substrate interface with consequent delamination), is attained at 0.795mm. The average scratching coefficient is about 0.71.

BN 46
B2
SS 440

The AE signal intensity and the sratching coefficient were plotted in Fig. 4 versus normal load between 0 and 70N. Plastic deformation begins at a load of 1.72N. Cracks along the edges of the track start at 6.25N. The first signs of delamination exposing the substrate, with transverse microcracks in the track and scattered BN debris appear at a load of 7.85N. At 14.32N the substrate within the track is totally exposed and some fine longitudinal striations appear along the edges of the scratch. The microcrack network is further developed with appearance of longitudinal and oblique microcracks. The last traces of BN in the track disappear at 21.13N. Striations continue until the end of the track. Transverse cracks become wider and more widely spaced towards the end of the scratch, as illustrated in the photomicrographs of Fig. 5.

Fig. 4 allows the approximate determination of the cohesive load L_C=6.75N, attained at 0.66mm from the beginning of the scratch and of the adhesive load L_A=8.06N, attained at 0.793mm. The average friction coefficient is about 0.78.

BN 47
B1
SS 17-4

The AE signal intensity and the scratching coefficient were plotted in Fig. 6 versus normal load between 0 and 70N. Microcracks along the edges of the track appear at a load of 2.7N. At 5.5N the first delamination of the coating appears at the edges of the scratch, as illustrated by the photomicrographs of Fig. 7. Transverse microcracks in the track within the BN coating and partially exposed substrate appear at 9.5N with debris scattered around the scratch. Transverse microcracks in exposed substrate appear at 11.5N. Longitudinal striations at the edges of the track appear at 17.3N and continue until the end of the scratch, at 70N. Large transverse cracks appear in the substrate within the track at 27.1N. They become wider and more widely spaced with increasing load until the end of the scratch. Figure 7e shows discontinuities in the BN coating unrelated to the scratch with exposure of the underlying substrate.

Figure 6 shows that L_C=5.12N attained at a distance of 0.512 mm from the beginning of the scratch and L_A=7.58N at 0.758mm. The average scratching coefficient is about 0.67.

BN 42
B2
SS 17-4

The AE signal intensity and the scratching coefficient were plotted in Fig. 8 versus normal load between 0 and 70N. Photomicrographs of the scratch are given in Fig. 9. With the beginning of te plastic deformation of BN the substrate is first exposed at the edges of the track at 1.97N. Tranverse microcracks within BN and coating delamination at the edges of the scratch appear at 6.12N. At 11.15N microcracks appear both in the coating and the exposed substrate and debris are scattered around the scratch. Transverse cracks within the denuded substrate and longitudinal striations which continue until the end of the scratch appear at 20.332N. Beyond 26.65N the transverse microcracks become very wide and widely spaced.

The cohesive load measured in Fig. 8 is L_C=5.00N at 0.506mm and the adhesive load L_A=7.05N at 0.714mm from the beginning of the scratch. The average scratching coefficient is about 0.74.

BN 48
B2
SS 17-4

The AE signal intensity and the scratching coefficient were plotted in Fig. 10 versus normal load between 0 and 70N. Photomicrographs of the scratch are shown in Fig. 11. Areas of exposed substrate were observed at the edges of the track in the plastically deformed coating at a load of 3.28N. Cracks appear at the track edges at 9.15N. Partially exposed substrate with transverse microcracks appear at a slightly higher load. Fully exposed substrate in the track and beginning of longitudinal striations are observed at 13.34N. They continue until the end of the sratch. The first wide crack appears at 21.89N. The spacing of these wide cracks increases and the cracks become wider towards the end of the scratch.

Fig. 10 shows that L_C=5.30N (at 0.532mm) and L_A=6.95N at 0.697mm from the beginning of the scratch. The average scratching coefficient is about 0.71.

Results are summarized in Table I. For comparison purposes Table II exhibits recently measured cohesive and adhesive loads of four coated specimens which were processed by various methods.

TABLE I

SUMMARY OF RESULTS

Specimen	L_C(N)	X_C(cm)	L_A(N)	X_A(cm)
BN47 B2 SS 440	6.29	0.616	8.05	0.795
BN46 B2 SS 440	6.75	0.66	8.06	0.793
BN47 B1 SS 17-4	5.12	0.512	7.58	0.753
BN42 B2 SS 17-4	5.00	0.506	7.05	0.714
BN48 B2 SS 17-4	5.30	0.532	6.95	0.697

TABLE II

ADHESIVE AND COHESIVE LOADS MEASURED ON OTHER COATINGS

TiB_2-coated MP35N nickel-base alloy (processed by fused salt electroplating)	L_C=7N	L_A=28N
(Al_2O_3-SiO_2-Cr_2O_3)-coated PH 17-4 steel (processed by batch CVD)	L_C=22N	L_A=38N
SiC-coated 4340 steel (processed by Plasma-Enhanced CVD)	L_C=17N	L_A=33N
TiN-coated PH 17-4 steel (processed by Cathodic Arc PVD)	L_C=31N	L_A=37N

Comparison of the above Tables clearly confirms the metallographic observations made on the coating surfaces and on the scratches that the BN coatings are very weak and adhere rather poorly to the stainless steel substrates.

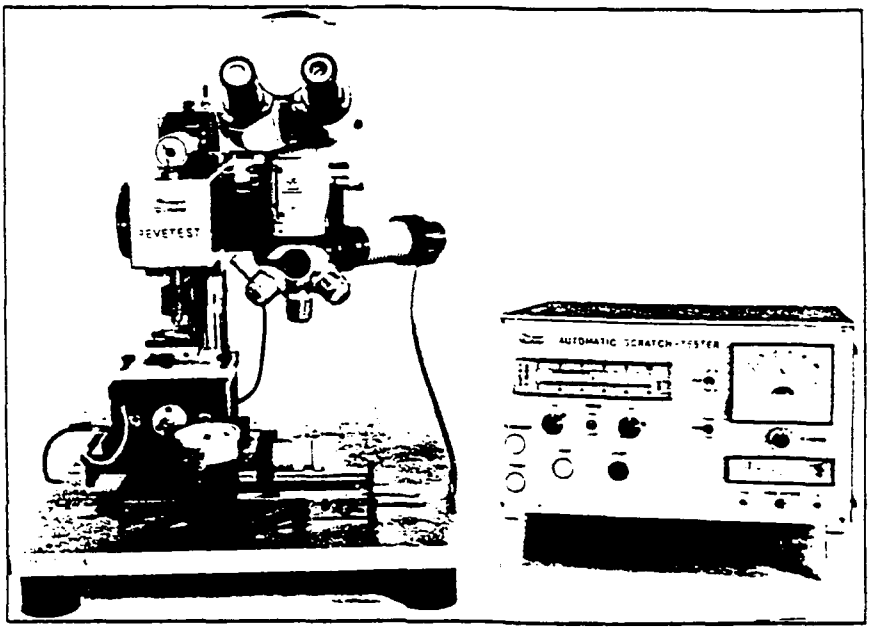

Figure 1: Revetest automatic scratch testing apparatus.

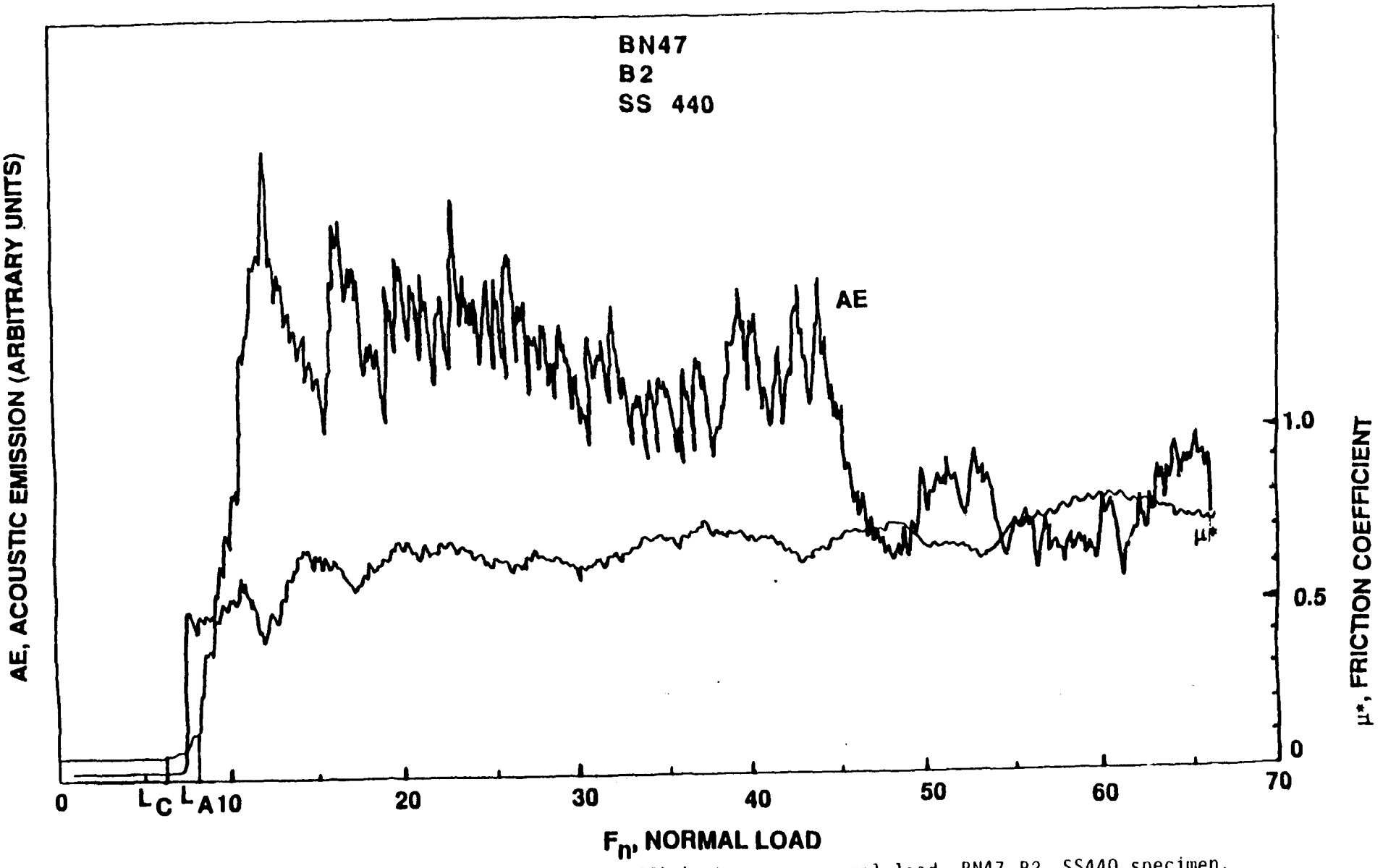

Figure 2: Acoustic emission and friction coefficient versus normal load. BN47,B2, SS440 specimen.

a

b

c

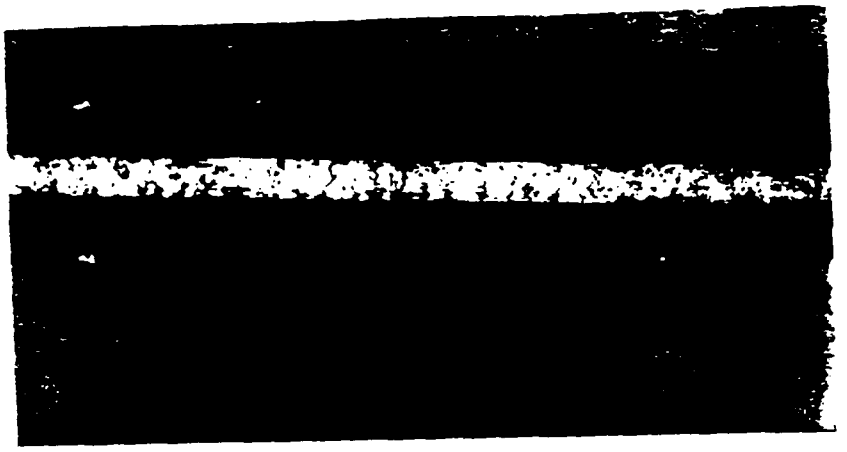

d

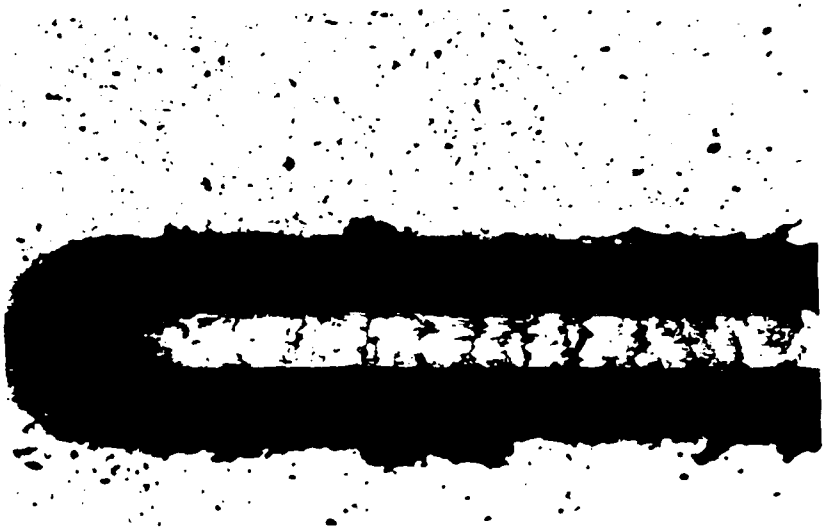

e

f

Figure 3: Photomicrographs of a scratch on coated specimen: BN47, B2, SS440. (a) to (e) 100X, (f) 375X.

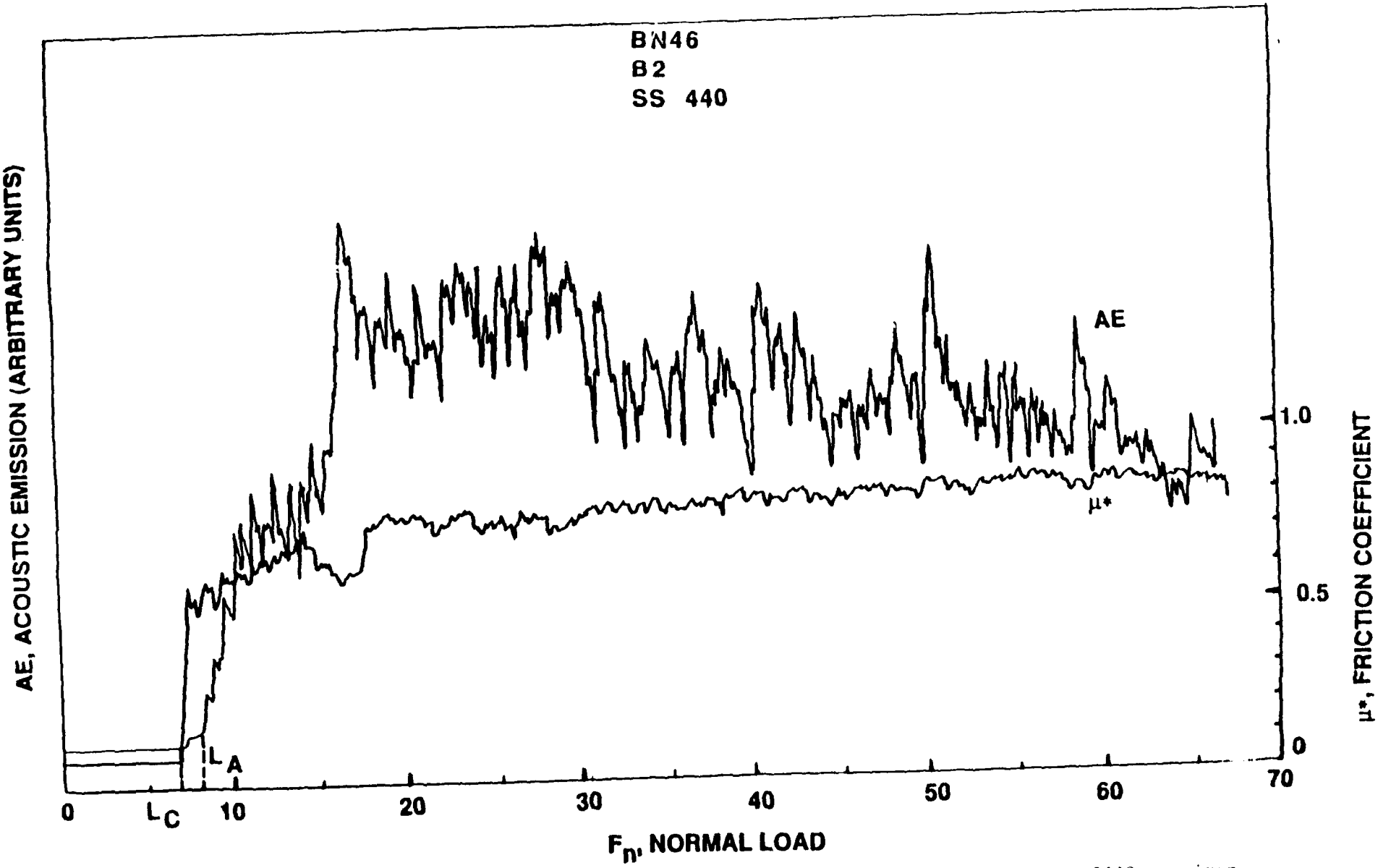

Figure 4: Acoustic emission and friction coefficient versus normal load. BN46,B2,SS440 specimen.

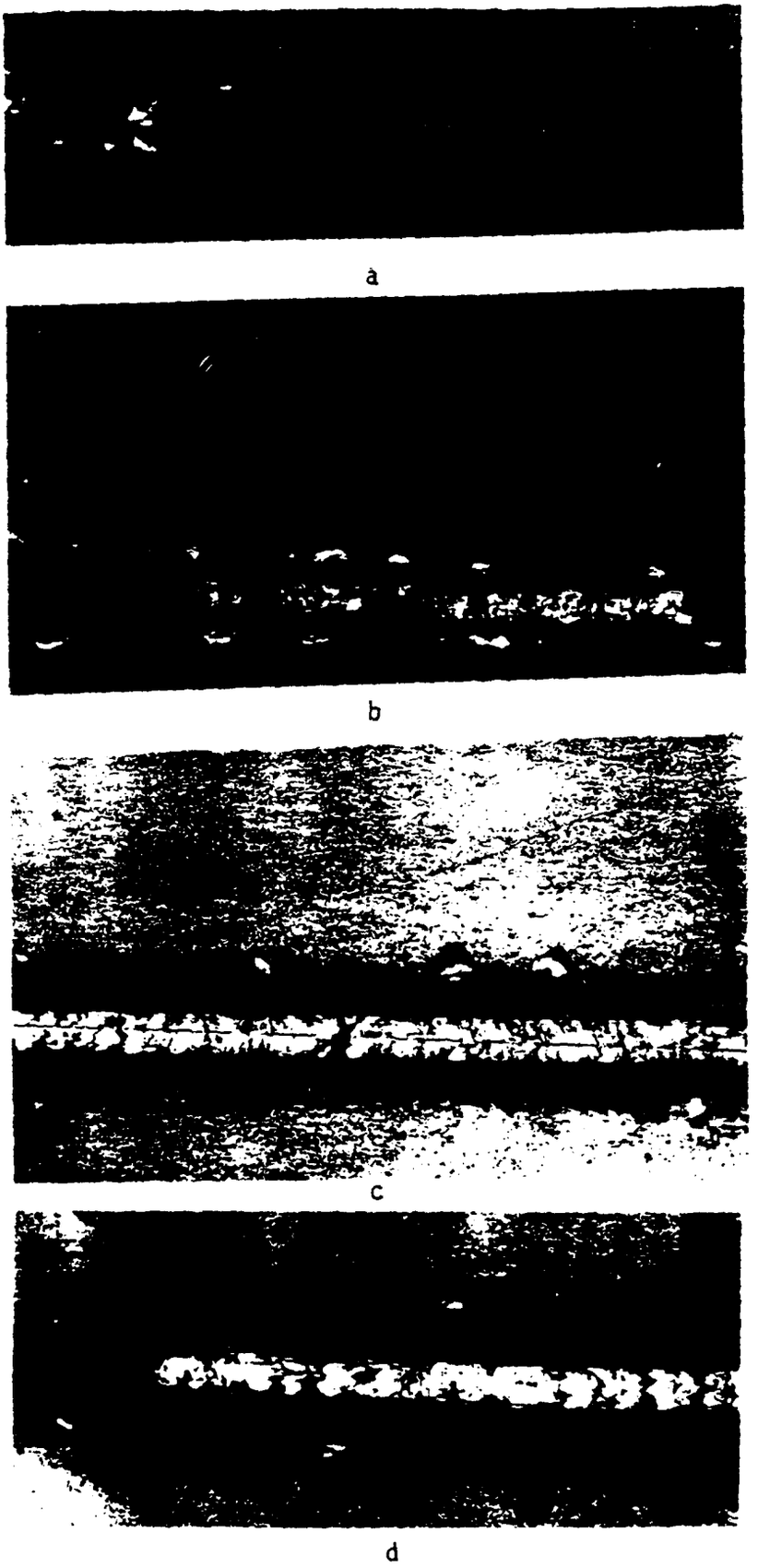

Figure 5: Photomicrographs of a scratch on coated specimen: BN 46, B2, SS440, 100X.

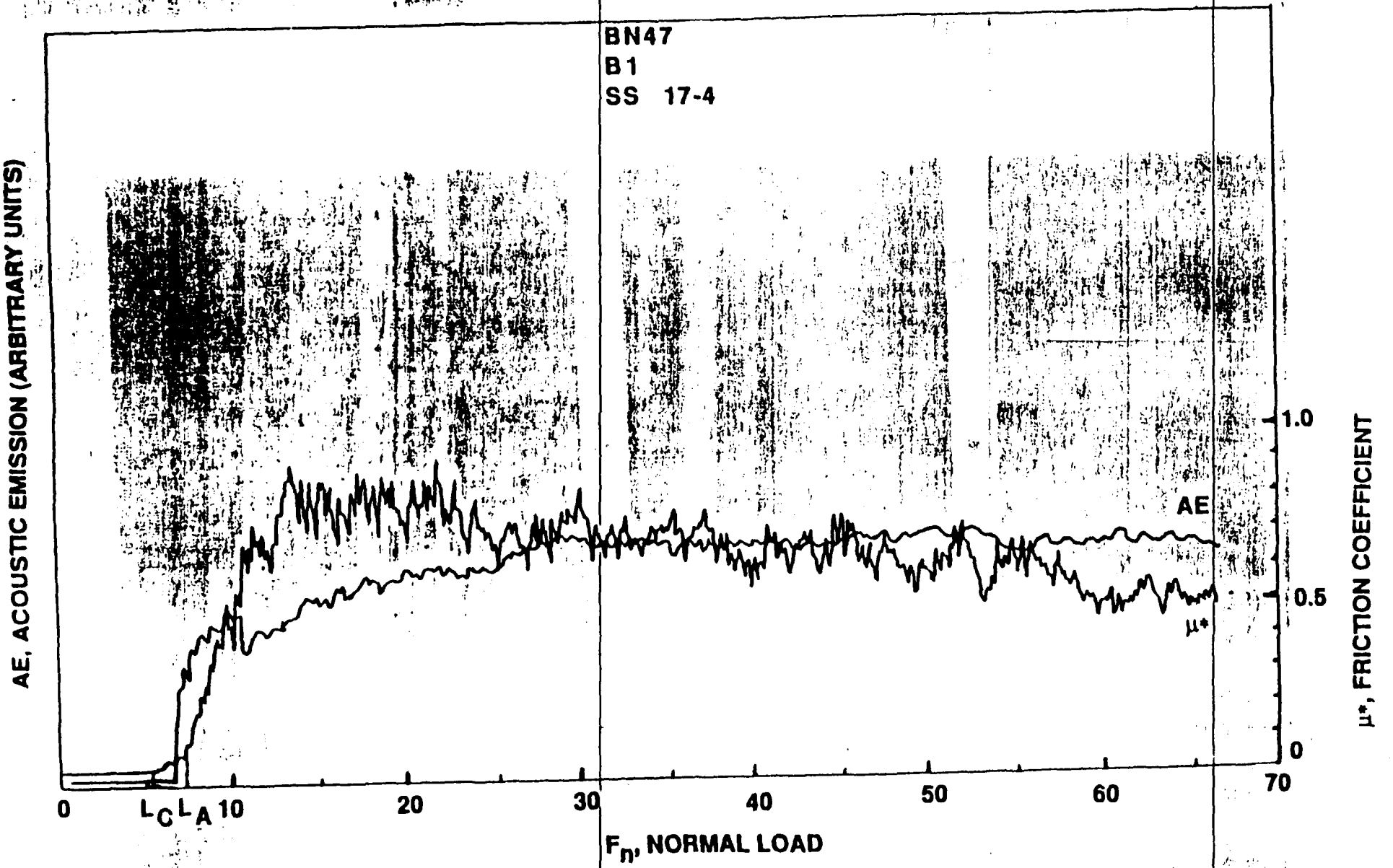

Figure 6: Acoustic emission and friction coefficient versus normal load. B47, B1, SS 17-4 specimen.

a

b

c

d

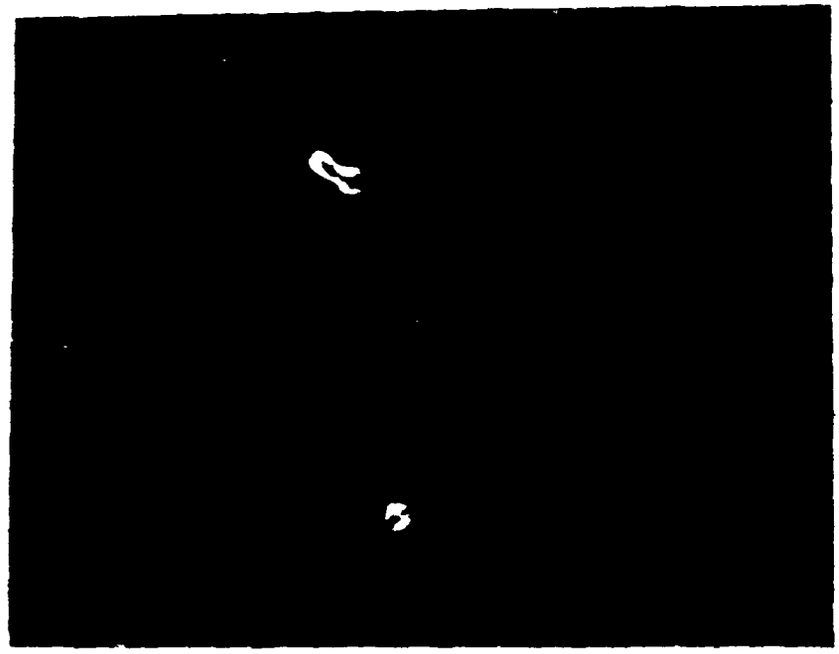

e

Figure 7: Photomicrographs of a scratch on coated specimen: BN 47, B1, SS 17-4.(a)-(d), 100X. (e)photomicrograph of defects on the coating surface, 100X.

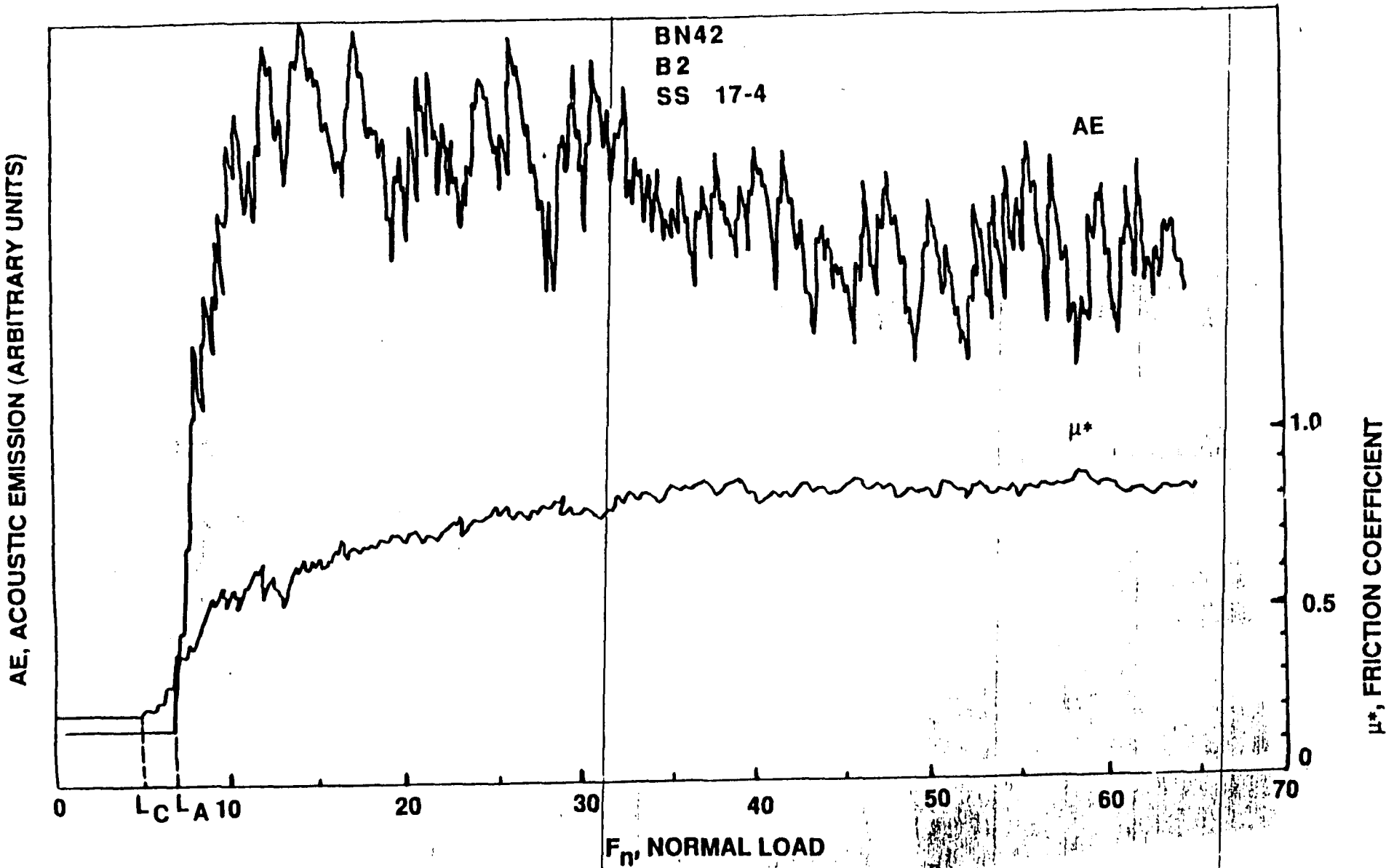

Figure 8: Acoustic emission and friction coefficient versus normal load. BN42, B2, SS 17-4 specimen.

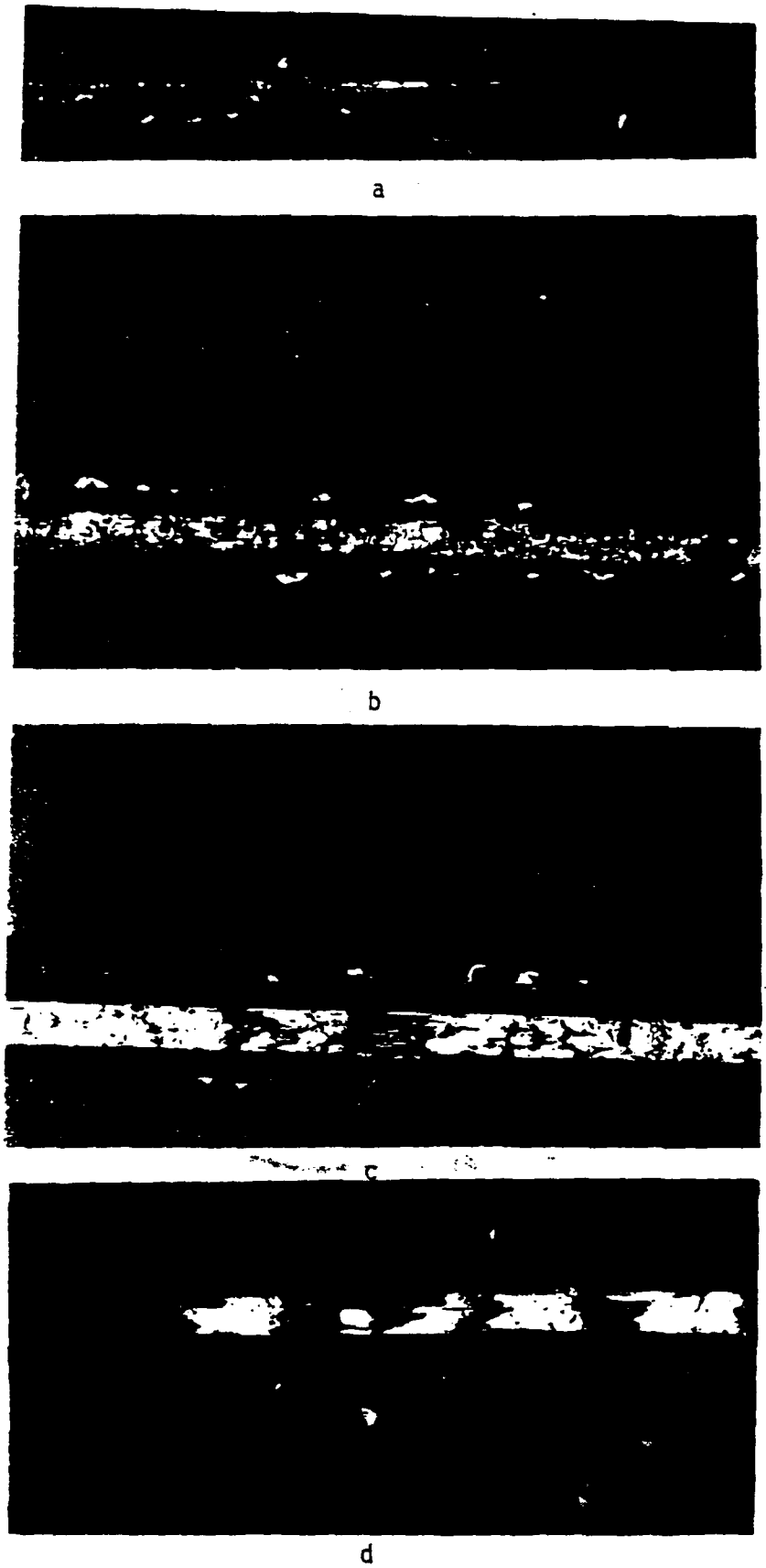

Figure 9: Photomicrographs of a scratch on a coated specimen: BN 42, B2, SS 17-4. 100X.

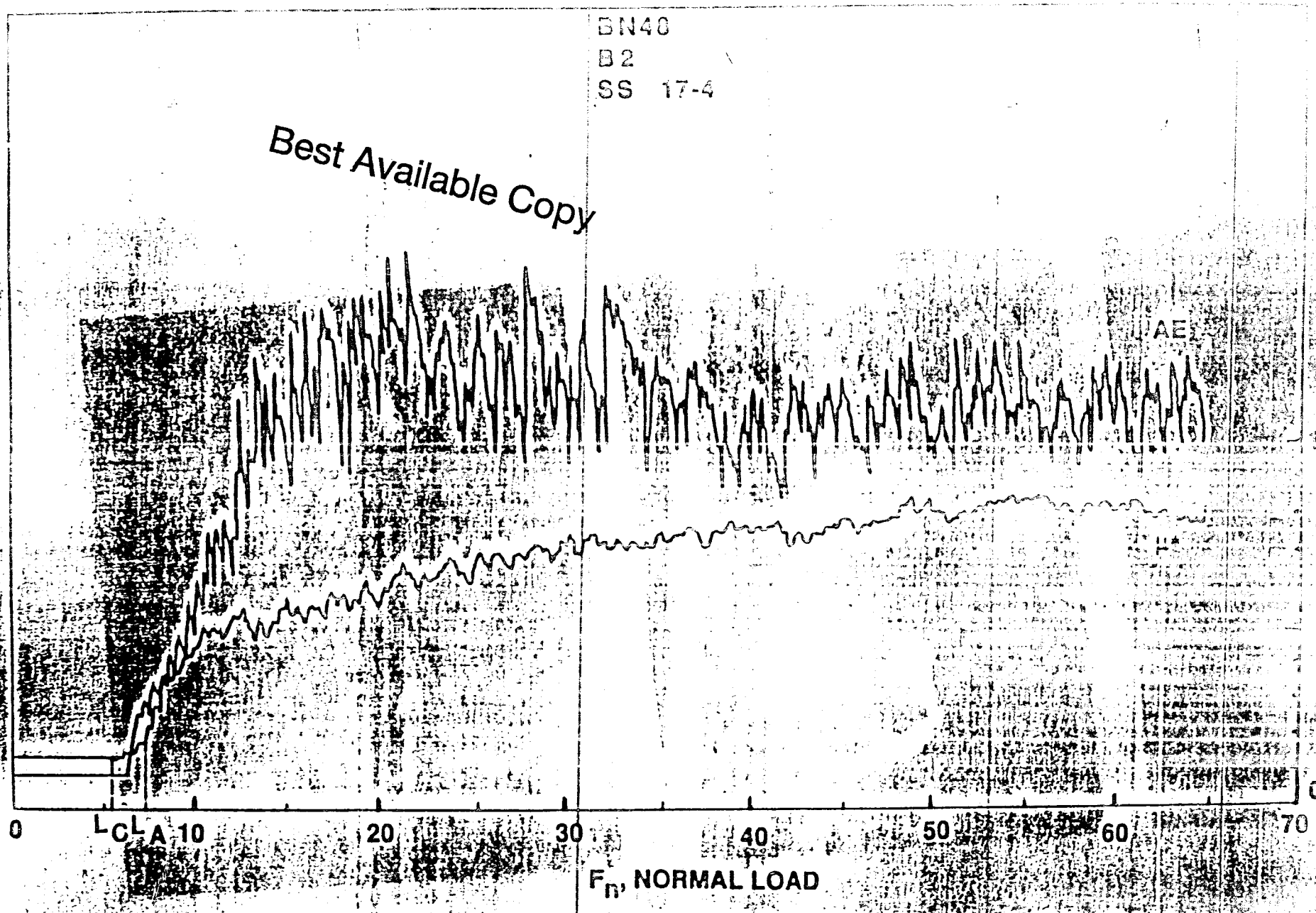

Figure 10: Acoustic emission and friction coefficient versus normal load, BN48, B2, SS 17-4 specimen

a

b

c

d

Figure 11: Photomicrographs of a scratch on a coated specimen: BN48, B2, SS 17-4, 100X.